Geological Society of America Bulletin

Multiple slope failures associated with neotectonic activity in the Southern Central Andes (37° –37°30'S), Patagonia, Argentina

Ivanna M. Penna, Reginald L. Hermanns, Samuel Niedermann and Andrés Folguera

Geological Society of America Bulletin published online 24 June 2011;
doi: 10.1130/B30399.1

Geological Society of America Bulletin, published online on 24 June 2011 as doi:10.1130/B30399.1

Multiple slope failures associated with neotectonic activity in the Southern Central Andes (37°–37°30′S), Patagonia, Argentina

Ivanna M. Penna[1†], Reginald L. Hermanns[2], Samuel Niedermann[3], and Andrés Folguera[1]
[1]*Laboratorio de Tectónica Andina, Departamento de Geología, Facultad de Ciencias Exactas y Naturales, Universidad de Buenos Aires, Ciudad Universitaria, pabellón II, 1427 Buenos Aires, Argentina*
[2]*Norges geologiske undersøkelse, Leiv Eirikssons vei 39, NO 7491 Trondheim, Norway*
[3]*Helmholtz-Zentrum Potsdam–Deutsches GeoForschungsZentrum, Telegrafenberg, D-14473 Potsdam, Germany*

ABSTRACT

Quaternary tectonic activity in the transition area between the Central and Patagonian Andes is closely associated with an anomalous cluster of rockslides: 19 rockslides with volumes up to 4 × 10^9 m^3 developed in plateau basalts. We divided them into two groups: (A) rockslides related to neotectonic activity and (B) rockslides not related to neotectonic activity. Thirteen rockslides, with a total volume of ~10 km^3, which lie on either folds or faults, have been displaced parallel to the structures and perpendicular to the valley axis, and they exhibit headscarps several kilometers away from the valley axis. Most of them are larger than 10^9 m^3, and are generally of rock avalanche type with a high degree of crushing of rocks, although local relief in some cases does not exceed 200 m. Nine rockslides with a total volume of 8.9 km^3 are related to folds, while four with a total volume of 1.3 km^3 are related to faults. The six rockslides not related to neotectonic activity have a total volume of 0.25 km^3 (of which the largest one accounts for 0.17 km^3), and are rotational slides and block topples with a low degree of rock fragmentation, although local relief is up to 400 m. The ^{3}He and ^{21}Ne surface exposure ages for six of these slides, as well as relative age assessment based on stratigraphic relation with glacial deposits and the drainage development on the rockslide deposit, suggest that the rockslide ages spread rather randomly between pre-glacial and mid Holocene, discarding climatic conditions as a common triggering factor. The absence of structures that can represent ideal sliding planes shows that rock fracturing due to neotectonic activity is a major conditioning factor for failures and that the magnitude of landslides is strongly controlled by the type of deformation.

INTRODUCTION

Based on a systematic analysis in the Alps, Abele proposed in 1974 the importance of tectonic activity as a preparatory mechanism for rockslides and suggested two relations: (1) "internal causes," referring to conditioning of rockslides by faults indicated by spatial coincidence of rockslides with the thrust faults, and (2) triggering by seismic activity. In the past years, systematic regional studies have investigated the strong link between the spatial relation of major rock avalanche clusters in several mountain belts and the control of tectonically related structures on the rockslide locations (e.g., Hermanns and Strecker, 1999; Redfield and Osmundsen, 2009). Other studies focused in more detail on the relation between large rock avalanche clusters and neotectonic settings with high complexity (Strecker and Marrett, 1999). A last group of studies focused on the exact way of conditioning of individual slides by neotectonic structures (e.g., Brideau et al., 2005; Martino et al., 2006). All of the studied sites have in common that large collapses were structurally preconditioned by major anisotropies dipping out of the slope. Based on temporal investigations of large rockslides in the NW Argentine Andes, Trauth et al. (2000) and Hermanns et al. (2006) showed that in addition to the neotectonic control on the location of rockslides, such events can also be controlled by climatic variability at least in narrow valley settings where river erosion directly causes slope undercutting.

Studies such as the one performed by Hovius et al. (1998) showed the active role of mass wasting in the erosion of young uplifting orogenic systems. Those authors suggested that during early stages of mountain uplift, tectonically controlled landslides contribute to the development of the drainage basins, while in later stages landslides only modify basins. In active tectonic areas of Asia, Europe, and America, Montgomery and Brandon (2002) observed that the uplift increases the frequency of landslides more than increasing the local relief. More recently, Molnar et al. (2007) suggested that rock fracturing by tectonic activity plays an important role for mountain erosion. With the study presented here we want to build on this observation and test whether tectonic fracturing also controls the locations of rockslides if ideal planes for sliding are missing and whether a difference of the style of tectonic deformation has an impact on the type, size, and total volume of rockslide activity in a mountain belt.

The eastern slope of the Andes between 36° and 38°S presents a high number of rockslides (Fig. 1; Escosteguy et al., 1999; Hermanns et al., 2004a; González Díaz and Folguera, 2005; González Díaz et al., 2006; Costa and González Díaz, 2007; Hermanns et al., 2011). Those collapses developed in Neogene flat-lying plateau basalts affected by the N-S–trending structures of the Guañacos fold-and-thrust belt (Folguera et al., 2004). The greatest relief in this region (~1000 m) was produced by W-E glaciofluvial valleys, which eroded into the plateau in the Quaternary. This conjunction of neotectonic structures (Quaternary activity) orthogonally cut by valleys laid the ground for an ideal natural laboratory for the study of the interactions between neotectonic, superimposed geomorphologic processes and the rockslide activity.

GEOLOGICAL SETTING

In the study area the main Cordillera has been uplifted since the late Miocene through the inversion of the Oligo-Miocene Cura Mallín Basin (Jordan et al., 2001). This occurred when the vector of convergence between the Nazca and South America plates became nearly orthogonal to the margin, and the convergence velocity increased from 55 mm/a to 138 mm/a (Pardo Casas and Molnar, 1987; Somoza and Ghidella, 2005). Oligo-Miocene rocks are represented by

†E-mail: penna@gl.fcen.uba.ar

 doi: 10.1130/B30399.1; 8 figures; 4 tables; Data Repository item 2011214.

Geological Society of America Bulletin, published online on 24 June 2011 as doi:10.1130/B30399.1

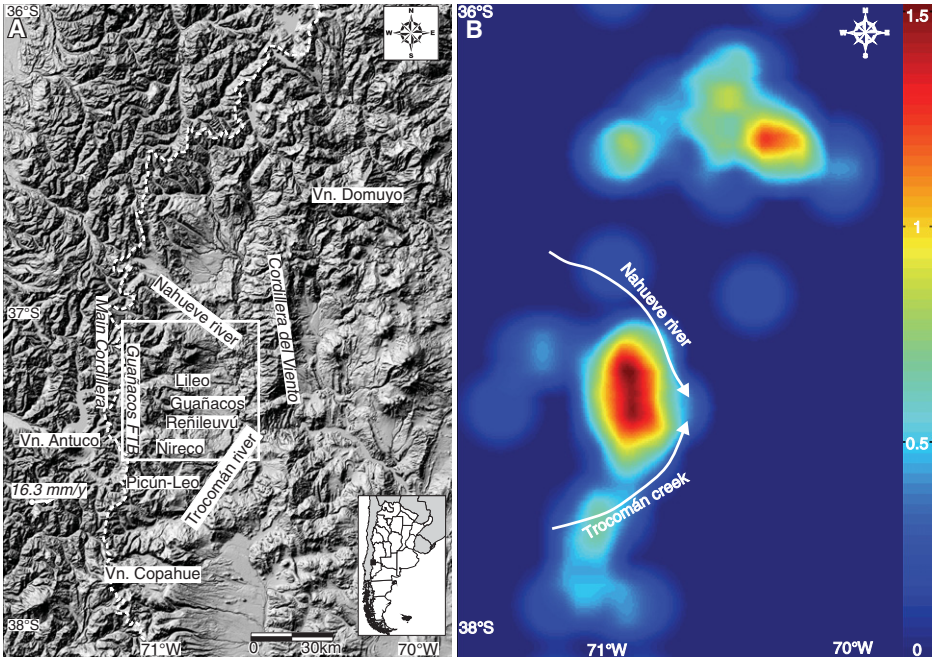

Figure 1. (A) Shaded image of the topography corresponding to the Andean drainage divide between 36° and 38°S, with indication of main geographical sites. Vn.—volcano; Guañacos FTB—Guañacos fold-and-thrust belt. The white box indicates location of Figure 2. (B) Density map of the same area showing concentration of rock avalanche phenomena between 36° and 38°S. Red colors indicate higher concentrations. Note that the highest rock avalanche concentration is located between the Lileo and Picún-Leo valleys.

the Cura Mallín Formation, which is composed of volcanic and sedimentary sequences (Jordan et al., 2001). This unit is paraconformably covered by the Mitrauquén Formation, a thick package of conglomerates dated by the whole-rock K-Ar method immediately west of the study area at 9–8 Ma (Suárez and Emparán, 1995). Both the Cura Mallín and Mitrauquén formations are covered with angular unconformity by the Plio-Pleistocene subhorizontal volcanic sequences of the Cola de Zorro Formation, which formed a volcanic plateau (Vergara and Muñoz, 1982). Between the Guañacos and Reñileuvú valleys (Fig. 1), Folguera et al. (2004) dated a lava flow at the top of this unit at 1.7 ± 0.2 Ma by whole-rock K-Ar.

During the Quaternary, fluvial courses and alpine glaciers eroded the plateau, creating valleys incised by ~200–1000 m. The best exposures of glacial deposits are lateral moraines located in the highest part of the plateau, at both margins of the Trohunco lake and at the northern margin of the Lauquén Mallín lake (Fig. 2). Based upon a detailed geomorphologic analysis of air photos, González Díaz and Folguera (2005) and González Díaz et al. (2006) classified the deposits in the area, distinguishing between glacial and rockslide deposits.

Due to the absorption of the plate displacements, most of the eastern Southern Central Andes are associated with neotectonic deformation (Costa et al., 2006). Global positioning system (GPS) measurements performed by Kendrick et al. (1999) show that the hinterland between 37° and 38°S is eastwardly transported (Fig. 1A). Recently, neotectonic activity has been described both in the forearc and western retroarc (Folguera et al., 2004, 2006; Melnick et al., 2006). Gravimetric models suggest that the subduction angle of the Nazca plate in this sector is ~10° shallower than in the adjacent segments both north and south, where it is ~30° (Tašárová, 2004). In the forearc and retroarc most of the seismicity is of interplate origin, with crustal events concentrated in the forearc (Bohm et al., 2002). However, some shallow events ranging from 3 to 5.6 M are located in the retroarc zone (U.S. Geological Survey [USGS]/National Earthquake Information Center [NEIC], 1973–present).

METHODOLOGY

Considering that the study area was partially glaciated, in the following we first reconstruct the glacial extents and focus thereafter on the neotectonic analyses and the description of the rockslides, including their absolute and relative dating. The latter is needed to test whether erosional processes related to glacial cycles are superimposed on the neotectonic control of rockslide activity.

Analysis of the Glacial Extent

To establish the maximum extent of ice and its retreat after the last glacial maximum, we first identified glacial landforms by air photo and satellite image interpretation. Additionally, five topographic profiles perpendicular to the valleys were constructed (Fig. 2), using as input the digital topography from Shuttle Radar Topographic Mission (SRTM, 90-m horizontal resolution and 10-m vertical accuracy). To support these observations, we analyzed the steepness of valley margins following Svensson's (1959) criteria. The author represented the valley cross section using a power law of the type $y = ax^b$, where y is the altitude of a point at distance x from the central line of the valley. The constant b is an index of the steepness of a valley margin, and a is a measure of the width of the valley floor. Values of b close to 1 indicate a margin close to a straight line, while values close to 2 indicate that the margin profile can be approximated by a parabola. The constant b was computed by the best fit of each side of each cross section to the model using the fit function from the Curve Fitting Toolbox for MATLAB, with the nonlinear least-squares method and trust region algorithm. Certain morphological features may generate convexities in the profile interfering with the determination of b, for instance the presence of terraces, taluses, or rockslide deposits. The profile locations that we selected for our determinations were chosen to avoid this problem (GSA Data Repository Table DR1[1]; Fig. 2).

Due to the small amount of glacial deposits in the study area, no studies were performed on the glacial extent during the last glacial cycles. We were only able to obtain one dateable sample of organic matter in glaciofluvial deposits which helped us to understand past glacial extents. The ^{14}C dating of organic material collected at 37°20′42.72″S, 70°53′30.90″W, 1210 m asl was performed by accelerator mass spectrometry (AMS) in the Leibniz Institute Kiel. This age is in good accordance to the reconstructed glacial extent in the valleys to the south.

[1]GSA Data Repository item 2011214, Additional tables and figures related to the maximum glacial extent, relative and absolute age of landslides deposits, and the program used to reconstruct the paleoslopes, is available at http://www.geosociety.org/pubs/ft2011.htm or by request to editing@geosociety.org.

Geological Society of America Bulletin, published online on 24 June 2011 as doi:10.1130/B30399.1

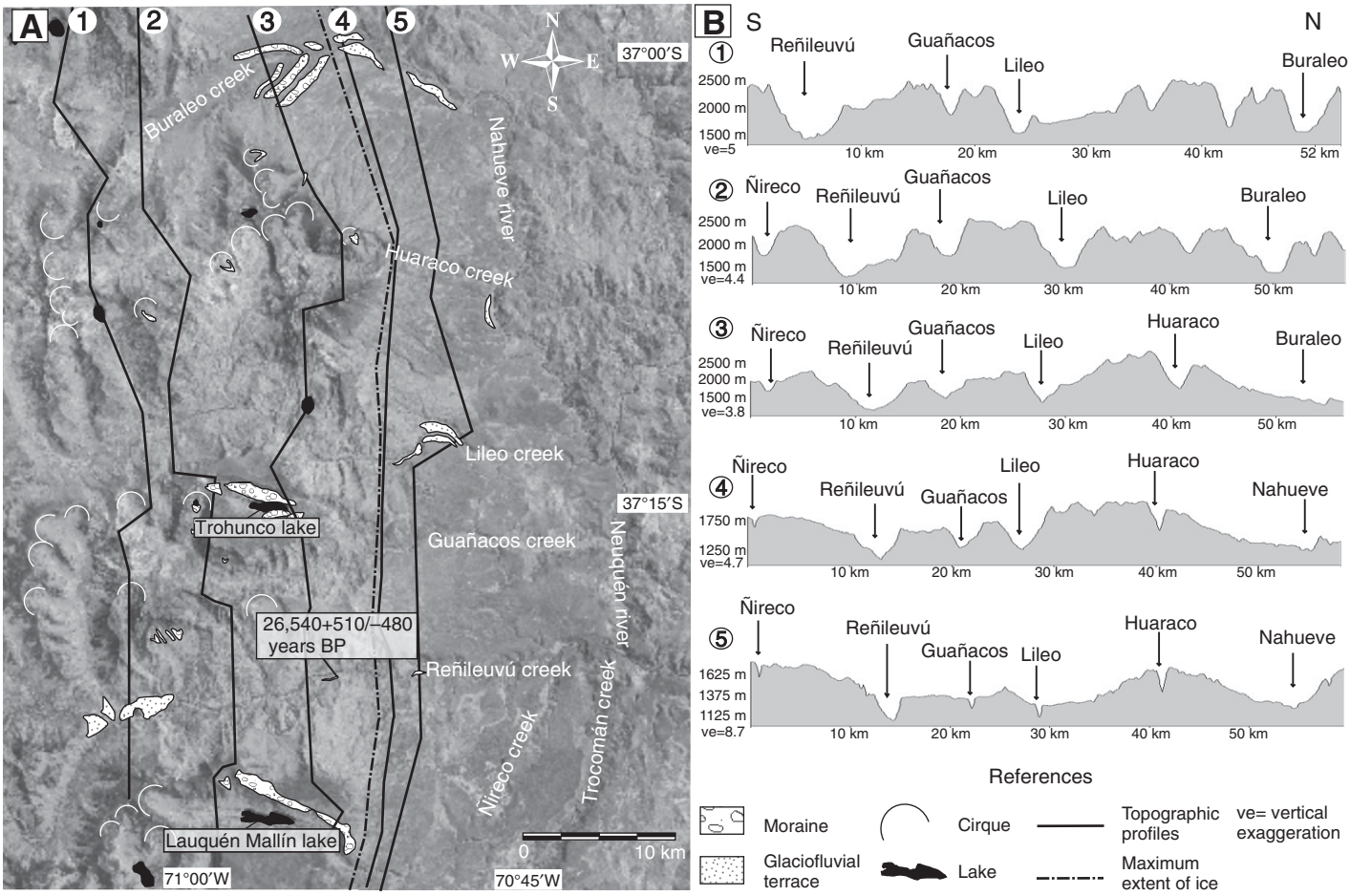

Figure 2. (A) Glacial and glaciofluvial landforms between the Buraleo and Ñireco valleys. Black lines labeled 1–5 indicate locations of topographic profiles shown in B. The age reported was established by ^{14}C dating of glaciofluvial deposits. (B) South-North trend topographic profiles across the valleys along lines shown in A. ve—vertical exaggeration.

Tectonic Analysis

Tectonic analysis was carried out first by air photo interpretation, considering drainage anomalies such as aligned springs, deflected courses, sag ponds, wind gaps, and topographic steps (Fig. 3). The features were then measured and described by direct field observation using discontinuities in the Quaternary cover.

In order to assess the contribution of the main structures to the present structural configuration, we constructed a restored cross section at 37°18′S (Table 1; Fig. 4). Structural and stratigraphic data collected by field work were compared to data from nearby localities (Suárez and Emparán, 1995; Jordan et al., 2001; Vietor and Echtler, 2006). Due to the lack of seismic lines or well-log data to provide information about the structural configuration at depth, we base our subsurface structural interpretation on the study of Jordan et al. (2001). These authors interpreted a seismic line (YPF 11128) 36 km farther north and proposed that the structures are mainly east-vergent, and the shortening is accommodated by inversion of the Cura Mallín Basin.

The restored section was built with a W-E strike, orthogonal to the structures (N-S), and following the principles outlined in the classic literature (Dahlstrom, 1969; Marshak and Woodward, 1988). Its restoration using line length allowed the calculation of a minimum shortening estimate and served to test the validity of the proposed model. Based on the same structural model, Vietor and Echtler (2006) constructed a regional restorable deformed composite section between 37.5° and 38°S from 71° to 69°W, which allows us to compare our results.

Rockslide Analysis

All rockslides were identified systematically by interpretation of air photos with a scale of 1:50,000 and satellite images as well as field mapping (Table DR2 [see footnote 1]) and were compared to previous studies (González Díaz et al., 2006). The rockslide density (Fig. 1B) was computed with the compilation of all rockslides from 36°–38°S and 70°–71°30′W. The area was divided in a squared grid, with 10 × 10-km cell size. The number of rockslides in each cell was computed, thus providing the density distribution. The calculations were carried out using MATLAB software.

Morphologic parameters of rockslides were calculated using the SRTM data (Table 2). Drainage density was computed as the ratio of the total length of courses that dissect the deposit to the deposit area (Table DR3 and Fig. DR1 [see footnote 1]). To estimate the volume of rock collapsed from the slope, we reconstructed a "paleoslope" by linear interpolation between the sides not affected by the collapse. The interpolation process is iterative. At each step, the height of every point belonging to the area to be interpolated is set as the average of the height of

Geological Society of America Bulletin, published online on 24 June 2011 as doi:10.1130/B30399.1

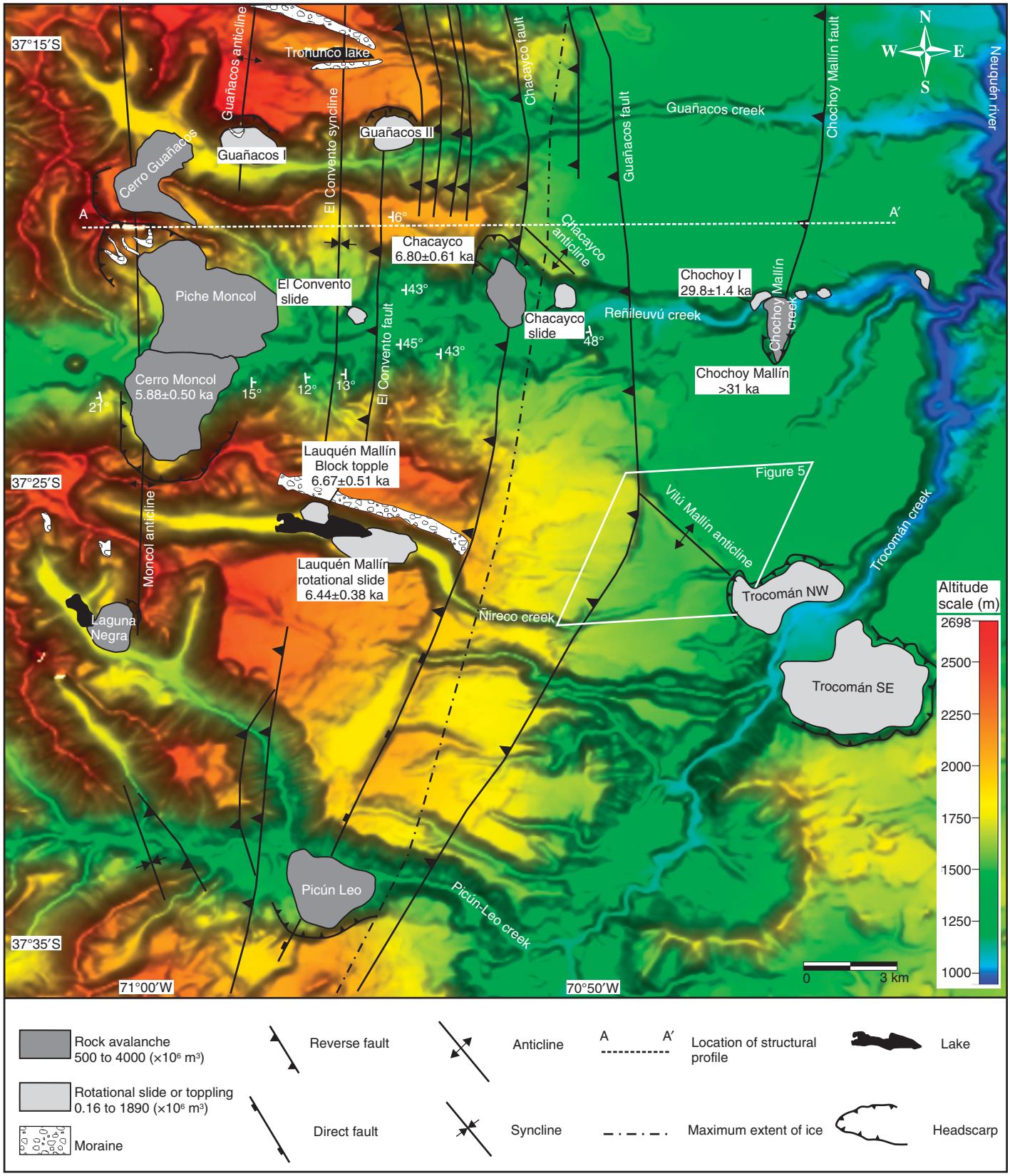

Figure 3. Spatial and temporal distribution of rockslides, locations of main neotectonic structures, and limit of ice extension during last glaciation. Structures in Guañacos and Picún-Leo valleys were taken from Folguera et al. (2006 and 2004, respectively).

Geological Society of America Bulletin, published online on 24 June 2011 as doi:10.1130/B30399.1

TABLE 1. MAIN CHARACTERISTICS OF THE STRUCTURES OBSERVED ALONG THE REÑILEUVÚ VALLEY FROM WEST TO EAST

Tectonic structure	Mechanism	Strike	Dip	Topographic vertical relief in top of the Quaternary coverage (m)	Total displacement (km)	Shortening (km)
Moncol anticline	Folding	N-S	65°W	Absent		0.70
El Convento syncline	Folding	N-S	64°W	Absent		
El Convento fault	Reverse faulting	N-S	75°W	Absent	0.625	0.36
Chacayco fault	Reverse faulting	NNE-SSW	68°W	400	3.550	1.36
Guañacos fault	Reverse faulting	N-S	55°W	30	2.500	1.45
Chochoy Mallín fault	Reverse faulting	N-S	58°W	15	1.125	0.95

its neighbors. The iteration continues until the heights converge. Calculations were carried out using a MATLAB custom routine (linear interpolation process program file [see footnote 1]). We determined the detached volume as the difference between the paleoslope and the present topographic conditions in the headscarp.

^{3}He and ^{21}Ne Surface-Exposure Dating of Rockslides

Because the concentration of cosmogenic nuclides in a surface rock depends on the duration of exposure to cosmic rays, its determination provides a powerful tool in Quaternary geochronology in general and for dating rockslides in particular (Ballantyne et al., 1998; Hermanns et al., 2001; Hermanns et al., 2004b; Cossart et al., 2008; Dortch et al., 2009; Antinao and Gosse, 2009 and references therein). In this study, we established 12 new surface-exposure ages of rock boulders in rock avalanche deposits of the Reñileuvú and Ñireco valleys based on cosmogenic ^{3}He and ^{21}Ne in pyroxene and olivine separates (Table 3). Sample sites were carefully chosen on air photos, selecting places far from trunk streams and in stable zones of the deposits. For sampling, only boulders larger than 1 m in diameter were selected, because they have most likely remained in the original exposure conditions since deposition, and thus since their first exposure to cosmic rays, without reworking. Boulder locations were determined with handheld GPS equipment. Three to five centimeters of flat-lying surfaces on the boulders were sampled. We measured the horizon shielding at each site in 30° steps. Similar to Ballantyne et al. (1998) or for multiple sites in Antinao and Gosse (2009), two boulders were sampled from each deposit. Pyroxene and olivine concentrates were produced based on magnetic properties and density contrast, and finally pure samples were handpicked under a stereo microscope. Noble gas analysis was carried out by stepwise heating in two or three steps up to 1750 °C at Deutsches GeoForschungsZentrum (GFZ) in Potsdam according to procedures described earlier (Niedermann et al., 1997; Kounov et al., 2007). The complete He and Ne results are presented in Table DR4 (see footnote 1).

Cosmogenic ^{3}He concentrations in pyroxenes and olivines are usually calculated by correcting the measured He for a magmatic component, the ^{3}He/^{4}He ratio of which is obtained by crushing the mineral grains in vacuo (e.g., Niedermann, 2002). However, for rocks older than a few tens of thousands of years, this method is not reliable because it does not account for radiogenic ^{4}He produced by U and Th decay (Blard and Farley, 2008). Therefore, U and Th concentrations have been determined by inductively coupled plasma–mass spectrometry (ICP-MS) at GFZ Potsdam in the host-rock matrix of all but two samples, and additionally in the pyroxene phenocrysts of six samples; results are shown in Table DR5 (see footnote 1). Assuming a crystallization age of 1.7–5.5 Ma (Folguera et al., 2004) and an average phenocryst grain size of 250 µm and using Equation (2) of Blard and Farley (2008), we expect radiogenic ^{4}He concentrations of ~13–77 × 10^{-8} cm^{3} STP/g in the pyroxene, and an estimated factor of 2 less in the olivine sample 190303-04. In comparison, measured ^{4}He concentrations are only ~5–19 × 10^{-8} cm^{3} STP/g in the pyroxenes and 0.9 × 10^{-8} cm^{3} STP/g in the olivine (Table DR4 [see footnote 1]), indicating only partial retention of the radiogenic ^{4}He as is quite commonly observed. However, the contribution of magmatic He is probably very small. This assumption is confirmed by the crushing extractions of four pyroxene separates (Table DR4 [see footnote 1]), which yielded very low He concentrations between 0.027 × 10^{-8} and 0.061 × 10^{-8} cm^{3} STP/g, respectively. Therefore, and because radiogenic He is virtually free of ^{3}He, we use total ^{3}He concentrations for the cosmogenic component. Cosmogenic ^{21}Ne concentrations, on the other hand, were determined from the ^{21}Ne excesses over atmospheric composition because crushing data were atmospheric (Table DR4 [see footnote 1]), and stepwise heating data were consistent with the air-cosmogenic mixing line for pyroxene ("spallation line"; Schäfer et al., 1999) in a three-isotope plot (Fig. DR2 [see footnote 1]).

To obtain exposure ages from cosmogenic nuclide concentrations, the production rates for the respective location and mineral chemistry have to be known. We calculated ^{3}He and ^{21}Ne production rates at sea level and high latitude (Table 3) according to Fenton et al. (2009) for each sample depending on the chemical composition (Table DR5 [see footnote 1]) and scaled them to the sampling altitude and latitude after Stone (2000). The ^{3}He production rates used are within the uncertainty range of the global mean as recently reported by Goehring et al. (2010). Correction factors (Table 4) were applied for horizon shielding (<2%), boulder size and geometry (Masarik and Wieler, 2003; ≤8%), and snow cover (<4%; see below). A conservative uncertainty estimate of 5% was assigned to the total correction factor (Table 3), reflecting the estimated precision to which these corrections can be assessed; a reduced 2% uncertainty was applied for those two samples with total correction factors close to 1 (210303-10 and -11; Table 3).

Because of the lack of accurate meteorological data, annual snow-cover estimates were provided by local inhabitants and were compared to data from the closest weather station. We estimated the number of months with snow cover per year and the average snow depth during those months for each sampling location (Table 4). We assumed that the boulders higher than the average snow depth most likely stick out of the snow throughout the year, with a minor cover for only a few days due to the strong winds in the area. The average snow density was chosen as 0.4 g/cm^{3} and the cosmic-ray spallation attenuation length as 167 g/cm^{2}.

The resulting surface-exposure ages are shown in Table 3. We only report Ne data for samples with ages >10 ka, because for the Holocene samples uncertainties of cosmogenic ^{21}Ne concentrations are very large, between 20 and >100%; otherwise the agreement of ^{3}He and ^{21}Ne ages is excellent. The error limits (95% confidence level) do not include systematic uncertainties of production rates and scaling, which are estimated at 10%–15%, because they only affect absolute ages but not the distribution of ages in a restricted area relative to each

Geological Society of America Bulletin, published online on 24 June 2011 as doi:10.1130/B30399.1

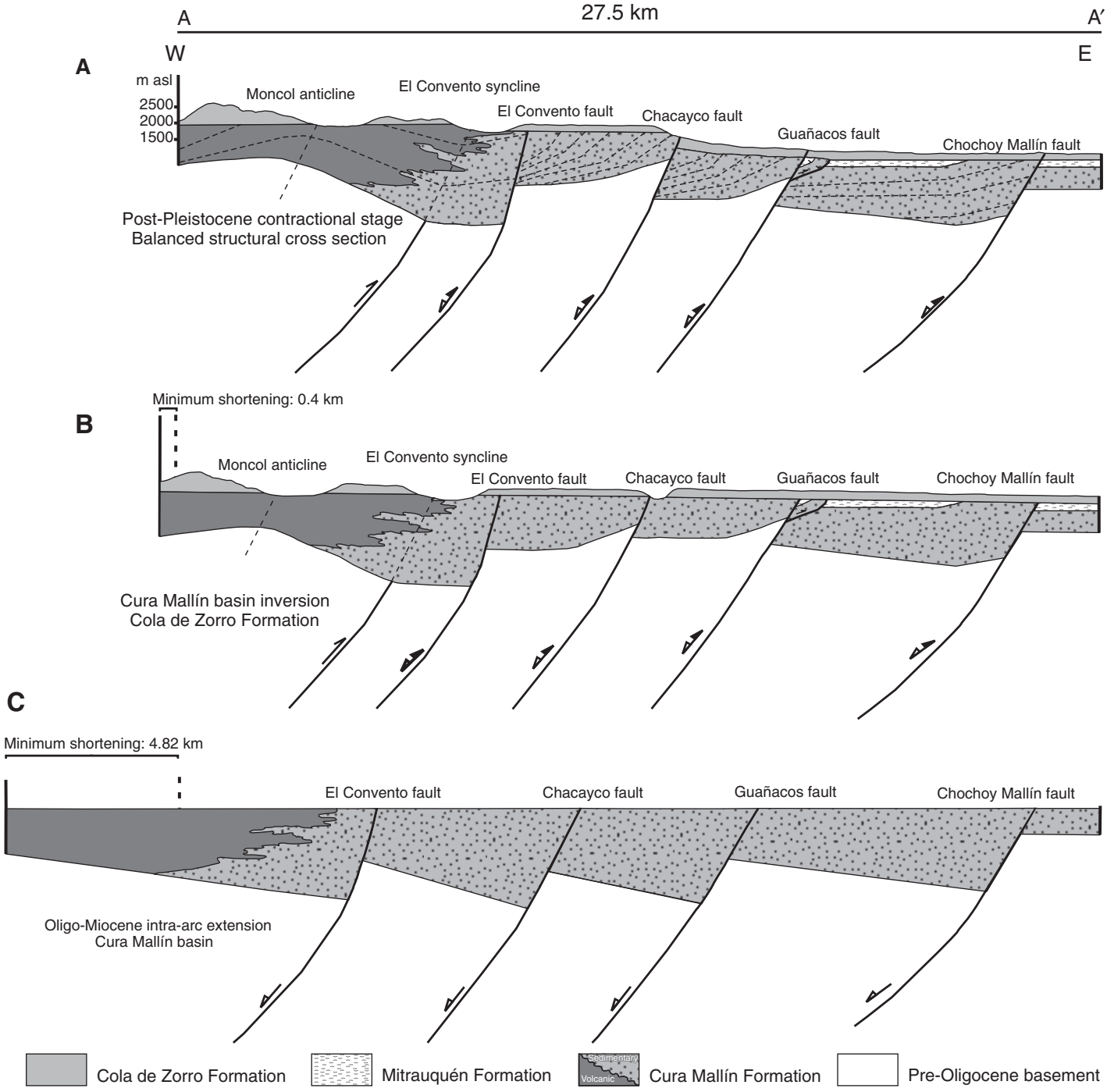

Figure 4. (A) Restored cross section with main episodes of deformation in the study area since Oligo-Miocene times. (B) Restoration to pre-contractional post-Pleistocene stage. (C) Restoration to pre-contractional Late Miocene stage, intra-arc extension. Note that the main reverse faults observed in the area correspond to the inversion of grabens from the Cura Mallín Basin. m asl—meters above sea level.

other. The ages shown in Table 3 are, however, minimum ages in the sense that erosion of the boulder surfaces was not taken into account. Indeed, erosion rates of ~1–2 mm/ka may be typical for the climatic and lithological setting of our study area (e.g., Costa and González Díaz, 2007). For samples with Holocene ages, such erosion rates would have a negligible effect of <1% on the exposure age. A 30-ka age would be increased by 6% and a 50-ka age by 10% at most. These corrections are likely overestimates for the stated erosion rate range, because the flat pattern of the cosmic-ray neutron flux on either side of the air-rock interface (Masarik and Reedy, 1995) will attenuate the effect of erosion as long as less than ~5 cm of rock have been removed from the surface, which will take 25 ka for a 2 mm/ka rate.

Geological Society of America Bulletin, published online on 24 June 2011 as doi:10.1130/B30399.1

TABLE 2. MASS WASTING DEPOSITS AND RELATED STRUCTURES IN THE REGION

Valley	Deposit	Type of movement	Relief scar/valley axis (m)	Volume ($\times 10^6$ m^3)	Distance scar/valley axis (km)	Relief/distance ratio	Structure related to	Age (ka)	Age reference
Guañacos	Guañacos I	Rotational slide	700	79	2.15	0.325	Guañacos anticline	>15–10*, <27	This study
	Guañacos II	Rotational slide	560	126	2.00	0.280	El Convento fault	<27†	This study
Reñileuvú	Piche Moncol	Rock avalanche	854	1340	7.14	0.119	Moncol anticline	>15–10*, <27	This study
	Cerro Moncol	Rock avalanche	789	4000	5.41	0.146	Moncol anticline	5.88 ± 0.50	This study
	Cerro Guañacos (Part I)	Rock avalanche	550	1150	2.74	0.201	Moncol anticline	<5–10†	This study
	Cerro Guañacos (Part II)	Rock avalanche	800	110	3.21	0.249	Moncol anticline	<15–10†	This study
	El Convento	Rotational slide	282	8	1.59	0.177	El Convento syncline	<27†	This study
	Chacayco	Rock avalanche	494	500	2.67	0.185	Chacayco fault	6.80 ± 0.61	This study
	Chacayco	Rotational slide	469	30	1.80	0.260	Chacayco anticline	<27†	This study
	Chochoy I	Rotational slide	140	5	0.73	0.192	Not related	29.8 ± 1.4	This study
	Chochoy Mallín	Rock avalanche	200	150	1.90	0.105	Chochoy Mallín fault	>31	This study
	Chochoy II	Rotational slide	139	0.3	0.44	0.316	Not related	<27†	This study
	Chochoy III	Rotational slide	142	0.16	0.54	0.263	Not related	<27†	This study
	Chochoy IV	Rotational slide	200	1.5	0.84	0.238	Not related	<27†	This study
Ñireco	Lauquén Mallín	Rotational slide	300	170	1.45	0.207	Not related	6.44 ± 0.38	This study
	Lauquén Mallín	Block topple	400	68	1.40	0.286	Not related	6.67 ± 0.51	This study
Picún-Leo	Laguna Negra	Rock avalanche	550	60	1.70	0.323	Moncol anticline	<27†	González Díaz and Folguera (2005)
	Picún-Leo	Rock avalanche	610	500	3.80	0.160	Chacayco fault	<27†	Folguera and Ramos (2002)
Trocomán	Trocomán (NW)	Rotational slide	420	340	2.50	0.168	Vilú Mallín anticline	<27†	This study
	Trocomán (SE)	Rotational slide	610	1890	6.14	0.099	Vilú Mallín anticline	<27†	This study

*Considering data from Rabassa et al. (2005) and Zech et al. (2008).
†Considering preservation degree of juvenile morphology and drainage density (Table DR3 [see footnote 1]).

LAST GLACIATION IN THE REGION

Glacial retreat is often proposed to contribute to slope collapses due to increasing relief or lateral stress release (Abele, 1974; Evans and Clague, 1994; Cossart et al., 2008). Since the late Miocene, the Southern Andes suffered repeated glacial cycles (Rabassa and Clapperton, 1990). During the last glacial maximum (LGM), an icesheet of ~440,000 km^3 extended along the Andes between 36°S and 52°S (Hulton et al., 1994). Whole-rock ^{40}Ar/^{39}Ar dating on lava flows performed by Singer et al. (2000) in the Laguna del Maule area (36°S, 70°30′W, 2200 m asl) indicates that the ice sheet retreated between 25.6 ± 1.2 and 23.3 ± 0.6 ka. Morphological analysis and dating (by cosmogenic ^{36}Cl) of the Varvarco rock avalanche deposit (36°26′S, 70°36′W) enabled Costa and González Díaz (2007) to show that these valleys have been ice free at 1900-m altitude prior to 30 ka. Based on whole-rock ^{40}Ar/^{39}Ar dating of lava flows from the Chillán volcano (37°S; Fig. 1A), Dixon et al. (1999) reported that the region was ice free at 25–30 ka. Similarly, dating of glaciofluvial deposits from the Copahue Volcano (37°50′S, 71°03′W, Fig. 1A) yielded an age of 30,000 ^{14}C yr B.P. (Bermúdez and Delpino, 1999). Based on ^{10}Be dating of moraine deposits in the Rucachoroi valley (39°S, Argentina), Zech et al. (2008) support the idea that a significant glaciation took place at 30–35 ka.

In the study area, the best exposures of glacial deposits are located in the lower section of the Buraleo creek, where there are three well-preserved frontal moraines (Fig. 2A). Likewise, at the northern margin of the Lauquén Mallín lake and at both margins of the Trohunco lake, we recognized lateral moraines 7 km and ~3.5 km long. We also recognized minor moraine deposits in the headwater area of the valleys and in two headscarps of rockslides (Figs. 2A and 3).

Using the Svensson (1959) method, we distinguished V-shaped from U-shaped cross sections between the Buraleo and Ñireco basins (Table DR1 [see footnote 1]; Fig. 2B). All valleys show an upper section dominated by glacial morphology and middle and lower sections with fluvial morphology. In the Huaraco, Lileo, Guañacos, and Ñireco valleys, this is reflected by a decreasing value of *b* when moving from the headwater toward the mouth (i.e., from profile 1 to profile 5 in Fig. 2B). In the Reñileuvú valley, the left side shows a similar trend to the valleys mentioned before, but on the right margin, the variation of *b* is less pronounced, due to the presence of taluses and erosion of that valley slope. In this valley, the profile 2 was discarded for the *b* determinations due to the presence of the Piche Moncol rock avalanche. The analyses allow us to conclude

TABLE 3. SAMPLING LOCATIONS, COSMOGENIC NUCLIDE CONCENTRATIONS, PRODUCTION RATES (P), AND RESULTING EXPOSURE AGES (T) OF PYROXENE (PX) AND OLIVINE (OL) SEPARATES FROM ROCKSLIDE BOULDERS IN THE REÑILEUVÚ AND ÑIRECO VALLEYS

Sample	Latitude (°S)	Longitude (°W)	Altitude (m)	$^{3}He_{tot}$ (10^{6} at/g)	$^{21}Ne_{ex}$ (10^{6} at/g)	Scaling factor*	Total correction factor†	P_3§ (at/g a)	T_3 (ka)	P_{21}§ (at/g a)	T_{21} (ka)
Cerro Moncol rock avalanche											
170303-10 px	37°22′0.54″	70°59′42.42″	1550	1.94 ±0.18	–	3.142	0.906	116.1	5.87 ±0.62	–	–
170303-11 px	37°22′0.42″	70°59′54.84″	1540	1.88 ±0.26	–	3.119	0.882	115.9	5.90 ±0.87	–	–
Chacayco rock avalanche											
170303-03 px	37°21′6.12″	70°52′12.72″	1260	1.90 ±0.19	–	2.537	0.932	114 ± 3	7.05 ±0.81	–	–
170303-04 px	37°20′56.7″	70°51′51.3″	1230	1.71 ±0.22	–	2.480	0.932	114 ± 3	6.49 ±0.91	–	–
Chochoy I rotational slide											
210303-10 px	37°21′1.02″	70°47′41.76″	1090	7.49 ±0.59	1.76 +0.25 –0.21	2.231	0.988	115.9	29.3 ±2.4	25.1	31.8 +4.6 –3.8
210303-11 px	37°20′28.68″	70°46′44.52″	1100	7.72 ±0.54	1.64 +0.25 –0.23	2.247	0.988	116.7	29.8 ±2.2	25.0	29.5 +4.5 –4.2
Chochoy Mallín rock avalanche											
170303-01 px	37°21′34.62″	70°46′25.08″	1190	12.9 ±1.0	2.97 +0.36 –0.32	2.407	0.908	116.6	50.6 ±4.7	26.4	51.5 +6.8 –6.1
170303-02 px	37°21′44.22″	70°46′13.02″	1080	8.45 ±0.59	2.11 +0.57 –0.42	2.214	0.953	116.4	34.4 ±3.0	26.3	38.0 +10.4 –7.8
Lauquén Mallín rotational slide											
190303-04 ol	37°25′58.32″	70°54′24.18″	1800	2.38 ±0.21	–	3.761	0.907	111.9	6.23 ±0.63	–	–
190303-06 px	37°25′58.44″	70°54′25.92″	1790	2.55 ±0.13	–	3.735	0.907	114.9	6.55 ±0.47	–	–
Lauquén Mallín block topple											
190303-01 px	37°25′16.02″	70°57′22.8″	1870	2.58 ±0.23	–	3.950	0.895	113.9	6.41 ±0.66	–	–
190303-02 px	37°25′13.8″	70°56′41.76″	1880	2.86 ±0.28	–	3.977	0.895	114 ± 3	7.05 ±0.80	–	–

*Calculated after Stone (2000).

†Total correction factors are the products of correction factors for horizon shielding, snow cover, and boulder geometry (Table 4) and have been assigned a conservative uncertainty of ± 5%, except for the Chochoy I slide (2%).

§^{3}He and ^{21}Ne production rates (P_3 and P_{21}) at sea level and high latitude are based on major element concentrations (Table DR5 [see footnote 1]) according to Fenton et al. (2009). For 170303-03, 170303-04, and 190303-02, P_3 was assumed to be similar to the other samples, with a conservative uncertainty included for the age calculation.

TABLE 4. CHARACTERISTICS OF SAMPLED BOULDERS AND CORRECTIONS APPLIED FOR AGE DETERMINATION

Sample	Boulder geometry	Snow cover*	Correction factor horizon	Correction factor snow cover	Correction factor boulder geometry
Cerro Moncol rock avalanche					
170303-10	2 × 1.5 m, rounded	30/4	0.986	0.977	0.940
170303-11	1.5 × 1 m, triangular profile	50/4	0.986	0.962	0.930
Chacayco rock avalanche					
170303-03	1 m, round	30/4	0.999	0.977	0.955
170303-04	1 m, round	30/4	0.999	0.977	0.955
Chochoy I rotational slide					
210303-10	15 × 20 m, flat	20/3	1	0.988	1
210303-11	6 × 5 m, flat	20/3	1	0.988	1
Chochoy Mallín rock avalanche					
170303-01	1 m, near circular shape	20/3	0.999	0.988	0.920
170303-02	2 × 2.5 m, rather flat	30/3	0.999	0.983	0.970
Lauquén Mallín rotational slide					
190303-04	1 m, round	50/5	0.997	0.953	0.955
190303-06	1 m, round	50/5	0.997	0.953	0.955
Lauquén Mallín block topple					
190303-01	2 m, cubic-trapezoidal	50/5	0.994	0.953	0.945
190303-02	2 m, cubic-trapezoidal	50/5	0.994	0.953	0.945

*x/y = Mean snow cover of x cm for y months a year

Geological Society of America Bulletin, published online on 24 June 2011 as doi:10.1130/B30399.1

that the easternmost extension of glaciers was at the longitude of profile 4 (Fig. 2B).

Due to the dynamics of the water courses, the glaciofluvial deposits are poorly preserved (Fig. 2A). At one locality in the Reñileuvú valley, these moderately consolidated, clast-supported conglomerate deposits could be dated by AMS to 26,540 + 510/–480 ^{14}C yr B.P. (KIA 22137). In agreement with other results from the region, we imply a glacial retreat not earlier than 27 ka. While alpine valleys were eroded during the last glacial maximum, we assign minor moraines located at altitudes higher than 2000 m asl to a minor glacial advance at ~15–10 ka as was proposed by Singer et al. (2000) for the Laguna del Maule (36°03′S, 70°29′W) area and by Rabassa et al. (2005) for the Patagonia region. Zech et al. (2008) reported a glacial advance at 11 ka based on cosmogenic ^{10}Be dating of a boulder in a cirque moraine in the Rucachoroi valley, 190 km to the south.

EVIDENCE OF QUATERNARY TECTONIC ACTIVITY

In the study area the Quaternary tectonic activity manifests itself as the Guañacos fold-and-thrust belt (Folguera et al., 2004). Stratigraphic and structural analyses suggest that two contractional deformation events must have taken place (Fig. 4; Jordan et al., 2001; Folguera et al., 2004). The first one generated the tectonic inversion of the Cura Mallín Basin (Jordan et al., 2001). We interpret the conglomerates of the Mitrauquén Formation recognized in this work (Fig. 5) as synorogenic deposits related to that event, as was suggested for this unit in the Mitrauquén locality by Suárez and Emparán (1997). The second one took place in post-Pleistocene times, producing the folding and faulting of the Cola de Zorro Formation (Folguera et al., 2004).

There are six major N-S structures in this area (Table 1; Figs. 3 and 4). In the following we describe them from W to E. The Moncol anticline defines the westernmost structure, while the Chochoy Mallín fault constitutes the easternmost one (Fig. 3). The restored cross section that we constructed allowed us to estimate a minimum shortening of 4.82 km since the onset of late Miocene contraction (Fig. 4). This is in the same order as concluded by Vietor and Echtler (2006) in a more regional study.

Moncol Anticline

In the Cerro Moncol area, volcanic strata from the Oligo-Miocene Cura Mallín Formation are folded in an anticline of 9 km wavelength by a blind thrust fault that generated a fault propagation fold with a western flank dipping 21°W and an eastern flank dipping 15°E (Figs. 3 and 4). The folded Cura Mallín layers are covered by subhorizontal lava flows and volcanic agglomerates from the Cola de Zorro Formation, and both sequences are intruded by subvertical dikes. Our restored cross section indicates that the structure that generated the Moncol anticline produced a minimum shortening of 0.7 km (Table 1; Fig. 4).

El Convento Syncline

The axis of this fold lies 5.7 km to the east of the Moncol anticline (Fig. 3). Volcanic and sedimentary strata from the Cura Mallín Formation are folded in a syncline of ~4 km semiwavelength with a western flank dipping ~15°E and an eastern flank dipping 13°W. We propose that the syncline is the result of the Moncol anticline to the W and the El Convento fault to the east (Fig. 4). The folded Cura Mallín layers are covered by subhorizontal layers from the Cola de Zorro Formation.

El Convento Fault

This fault is recognized along 20 km from north to south between the northern margin of the Guañacos valley and the southern margin of the Reñileuvú valley (Fig. 3). The El Convento fault deforms sedimentary and volcanic strata from the Cura Mallín Formation (Table 1; Fig. 4). West of this fault the Cura Mallín strata dip 13°W, while east of the fault they dip around 43°W. The Plio-Pleistocene volcanic cover has not been affected by this structure (Fig. 4).

Chacayco Fault

This fault is recognized along 80 km from north to south between the Lileo valley and the Copahue-Caviahue volcano (Table 1; Fig. 1A). In its middle section where it crosses the Reñileuvú valley, the fault puts sedimentary strata from the Cura Mallín Formation in contact with volcanic lavas, the top of which was K-Ar dated at 1.7 ± 0.2 Ma (Folguera et al., 2004). Activity of this fault generated a mountain front that reaches a maximum relative relief of 400 m (Fig. 4).

The Chacayco fault propagation fold has a NW strike and is exposed in the northern margin of the Reñileuvú valley, 1.8 km east of the interception of the valley and the Chacayco fault. This anticline is produced by a blind thrust fault affecting volcanic strata from the Cola de Zorro Formation (Fig. 3; Folguera et al., 2004).

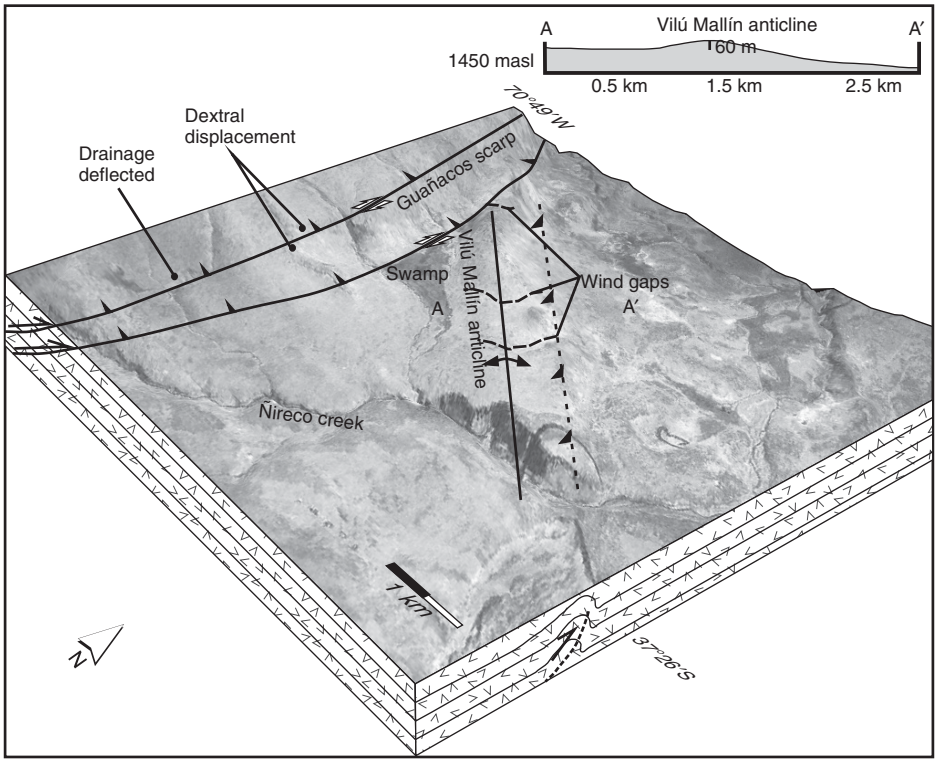

Figure 5. Block diagram showing Guañacos scarp and Vilú Mallín anticline and morphological features associated with them in the lower section of the Ñireco valley. Vertical exaggeration—1.5.

Geological Society of America Bulletin, published online on 24 June 2011 as doi:10.1130/B30399.1

Guañacos Fault

This fault is 43 km long, emerging from north to south between the Lileo and Picún-Leo valleys (Fig. 1A). It develops a rectilinear step of ~30 m in height in rocks from the Cola de Zorro Formation and the Quaternary sedimentary cover (Table 1; Fig. 4). Folguera et al. (2004) defined its mechanism as transpressive dextral, based on the finding of a 3.1 Ma lava flow dextrally displaced by 200 m. Along this scarp we recognized drainage disturbances such as abandoned courses, deflected courses, rectilinear courses, and aligned springs (Fig. 5). Related to this fault, a minor fault offsets conglomeratic strata of the Mitrauquén Formation in the southern margin of the Reñileuvú valley and puts them in subvertical position (Fig. 6).

Between the Reñileuvú and Ñireco valleys, a blind thrust fault generated the NW-SE Vilú Mallín anticline, oblique to the Guañacos scarp (Fig. 5). Three wind gaps evidence the variation of the drainage direction of a creek that drains a swamp by the growth of this structure. The Ñireco creek cuts this fold generating a deep gorge (Fig. 5).

Chochoy Mallín Fault

In the eastern edge of the Guañacos fold-and-thrust belt, the Chochoy Mallín fault exhumes lacustrine and volcanic sequences. A pyroclastic bed interspersed in the sedimentary deposit was dated by $^{40}Ar/^{39}Ar$ in hornblende at 22.8 ± 0.7 Ma (Jordan et al., 2001). The fault puts the Cura Mallín rocks in contact with the Plio-Pleistocene volcanic cover, resulting in a 15-m topographic step (Table 1; Fig. 4). The morphological features associated with this structure are more subtle than in the cases described before. Only the topographic discontinuity and some aligned ponds were observed between the Guañacos and Reñileuvú valleys.

MASS WASTING DEPOSITS

Nineteen rockslide deposits were mapped along the Guañacos, Reñileuvú, Ñireco, and Picún-Leo valleys (Tables 2 and DR2 [see footnote 1]; Fig. 3). All of these rockslides involved subhorizontal volcanic sequences. Seven are from the rock avalanche type, 11 are rotational slides, and one is a topple failure. We dated three rock avalanches and one rotational rockslide in the Reñileuvú valley and two rockslides in the Ñireco valley by surface-exposure dating using cosmogenic ^{3}He and ^{21}Ne. A relative age was assigned for the remaining deposits based on their relation with glacial deposits, the preservation degree of juvenile morphologies, the drainage density (Table DR3 and Fig. DR1 [see footnote 1]), and the degree of connection of depositional basins.

Rock-Slope Failures Lining Up along Active Structures

In the following we describe the rockslide deposits related to the different structures from W to E, proceeding from N to S along each structure (Fig. 3).

Rockslide Deposits along the Moncol Anticline

The Cerro Guañacos rock avalanche deposit has a volume of 1260×10^6 m^3. Digregorio and Uliana (1975) mapped it as a glacial deposit, but later González Díaz and Folguera (2005) analyzed its morphological features by aerial photo interpretation and assigned its origin to a rock avalanche. The rock avalanche deposit is composed of rocks of the Cola de Zorro and Cura Mallín formations. The deposit is divided in two lobes (Part I and Part II; Table 2), one lies in a tributary of the Reñileuvú creek in SE direction from the scarp, while the other lobe lies transversal to the Guañacos creek in S-N direction. Here the deposit shows a runup of 90 m on the northern slope of the valley (Fig. 3). The rock avalanche had split into two lobes when it occurred at the drainage divide between the Guañacos and the tributary of the Reñileuvú valleys. The deposit has a well-preserved juvenile morphology, lacking a continuous drainage system (Table DR3 and Fig. DR1 [see footnote 1]), with meter-sized volcanic blocks and pronounced hummocks on the surface suggesting a relatively young age (<15–10 ka).

Near the headwater of the Reñileuvú creek, the Piche Moncol and Cerro Moncol rock avalanche deposits are partially superposed (Fig. 3; González Díaz and Folguera, 2005 and Escosteguy et al., 1999, respectively). Both collapses involved volcanic sequences from the Cola de Zorro and Cura Mallín formations. The Piche Moncol rock avalanche (1340×10^6 m^3) originated in the northern slope of the valley (Table 2). In its upper part the deposit is covered by lateral and frontal moraine deposits. Incipient catchment areas have developed on its lower surface (Fig. 3) connecting depositional depressions on the surface of the rock avalanche deposit (Table DR3 and Fig. DR1 [see footnote 1]). In addition, hummocks are subdued and only a few meter-sized blocks emerge at its surface. A glaciofluvial cover of gravels ~7 m thick is exposed at the distal part of the deposit. Based on this morphologic

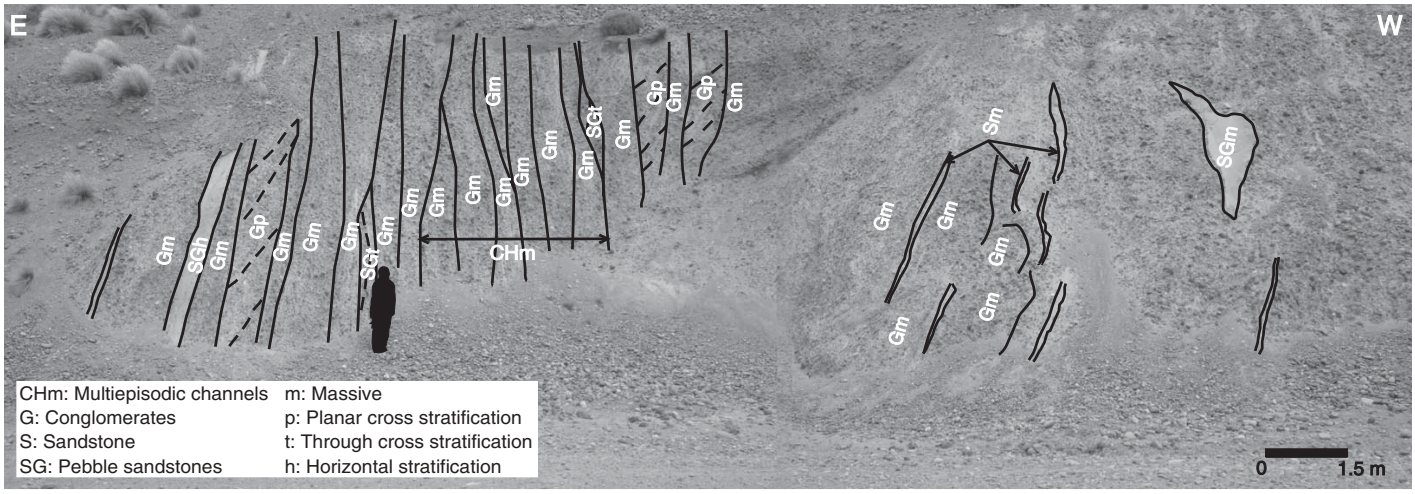

Figure 6. Conglomeratic Pliocene sequences outcropping at the southern margin of the Reñileuvú valley, downstream of Guañacos fault. Solid lines delimit channel deposits. Dashed lines represent stratification.

Geological Society of America Bulletin, published online on 24 June 2011 as doi:10.1130/B30399.1

evidence, we estimate an age younger than the maximum glacial extent (<27 ka) and older than last glacial readvances in the region (>15–10 ka).

The Cerro Moncol rock avalanche (4000 × 10^6 m^3) originated on the southern slope of the Reñileuvú valley, juxtaposed to the Piche Moncol rock avalanche (Table 2; Fig. 3). The morphology of the headscarp is very fresh, and it presently has small secondary slides, rock falls and debris flows. The deposit has a very well preserved hummocky topography with a disjoined drainage network and multiple lakes on its surface (Table DR3 and Fig. DR1 [see footnote 1]). Some hummocks of this deposit were emplaced over a fluvial terrace, indicating that the avalanche occurred during a fluvial stage after the maximum glacial extent. This deposit was dated by two ^{3}He ages of 5.87 ± 0.62 and 5.90 ± 0.87 ka, yielding an error-weighted mean of 5.88 ± 0.50 ka (Tables 2 and 3).

The Laguna Negra rock avalanche deposit (60 × 10^6 m^3) originated at the northern slope of the upper Picún-Leo basin (Table 2). The rock-avalanche deposit has dammed the valley, forming the Laguna Negra lake (Fig. 3; Hermanns et al., 2011). The deposit is juvenile with pronounced hummocks, and the drainage system on its surface is poorly developed, suggesting a Holocene age (Table DR3 [see footnote 1]).

Rockslide Deposits along the Guañacos Anticline

In the northern margin of the Guañacos valley, the Guañacos I rotational rockslide involved 79 × 10^6 m^3 (Table 2; Fig. 3). The presence of small moraines over the headscarp and the deposit allows us to estimate an age prior to 15–10 ka, however younger than the age of the maximal glacial extent (<27 ka) because the deposit lies in a section of the valley with glacial morphology, but does itself not exhibit any glacial disturbances.

Rockslide Deposits along the El Convento Fault

The Guañacos II rotational rockslide involved 126 × 10^6 m^3. It is composed of volcanic sequences, and it originated from the northern slope of the Guañacos valley (Table 2; Fig. 3). The age of this collapse is unknown, but considering the good degree of preservation of both the headscarp and the deposit indicating no glacial overprint, it is of postglacial age.

To the south and within the Reñileuvú valley, the El Convento rotational rockslide involved 8 × 10^6 m^3 volcanic rocks of the Cura Mallín Formation. The headscarp is located between the eastern end of the El Convento syncline and the El Convento fault (Table 2; Fig. 3). Considering the good degree of preservation of both the headscarp and the deposit not showing any signs of glacial overprint, the deposit is postglacial as well (<27 ka).

Rockslide Deposits along the Chacayco Fault

In the middle section of the Reñileuvú valley, the Chacayco rock avalanche (Hermanns et al., 2011) involved 500 × 10^6 m^3 from the Cola de Zorro and Cura Mallín formations (Table 2; Figs. 3 and 7). The rock mass was displaced perpendicular to the valley axis, generating a runup of 80 m in the southern margin and producing a semiconfinement of the Chacayco creek (Fig. 3). On top of this deposit a semiconnected drainage network has developed (Table DR3 [see footnote 1]) with very well preserved hummocks. Several meter-sized blocks cover its surface. This deposit was dated with two ^{3}He ages of 7.05 ± 0.81 and 6.49 ± 0.91 ka, yielding an error-weighted mean of 6.80 ± 0.61 ka.

The Picún-Leo rock avalanche (500 × 10^6 m^3) originated 26 km to the south of the Chacayco rock avalanche, in the Picún-Leo valley (Fig. 3; Hermanns et al., 2011). Folguera and Ramos (2002) assigned this movement to postglacial times based on stratigraphic relations.

Rockslide Deposits along the Chacayco Anticline

The Chacayco rotational rockslide is composed of 30 × 10^6 m^3 volcanic rocks of the Cola de Zorro Formation (Table 2; Fig. 3). Its headscarp is well preserved and concave upward. Based on the juvenile morphology, we estimate a postglacial age for the deposit (<27 ka).

Rockslide Deposits along the Chochoy Mallín Fault

In the eastern extreme of the Guañacos fold-and-thrust belt, the Chochoy Mallín rock avalanche (150 × 10^6 m^3) originated at ~1250 m asl, near the mouth of the Reñileuvú creek (Table 2; Fig. 3). West of the headscarp of the Chochoy Mallín rock avalanche the Chochoy Mallín creek drains in WSW-ENE direction and suddenly turns to S-N direction, developing an elbow of ~110°. East of the scar, an abandoned channel has remained, reflecting that prior to the slope collapse the creek drained almost parallel to the Reñileuvú (W-E direction) into the Ñireco creek, indicating that this creek was captured after the collapse. The rock avalanche deposit has subdued morphology, and a well- to moderately developed drainage system has established on its surface (Table DR3 and Fig. DR1 [see footnote 1]). Two boulders on this deposit were dated with cosmogenic ^{3}He and ^{21}Ne. While ^{3}He and ^{21}Ne ages agree for each boulder (Table 3), the mean values for the two boulders are considerably different at 50.9 ± 3.8 and 34.8 ± 2.9 ka, respectively (see Discussion).

Rockslide Deposits along the Vilú Mallín Anticline

In a regional geological map, Digregorio and Uliana (1975) interpreted two deposits at both sides of the middle section of the Trocomán valley as moraines. However, those deposits occur beyond the maximal glacial extent in the region

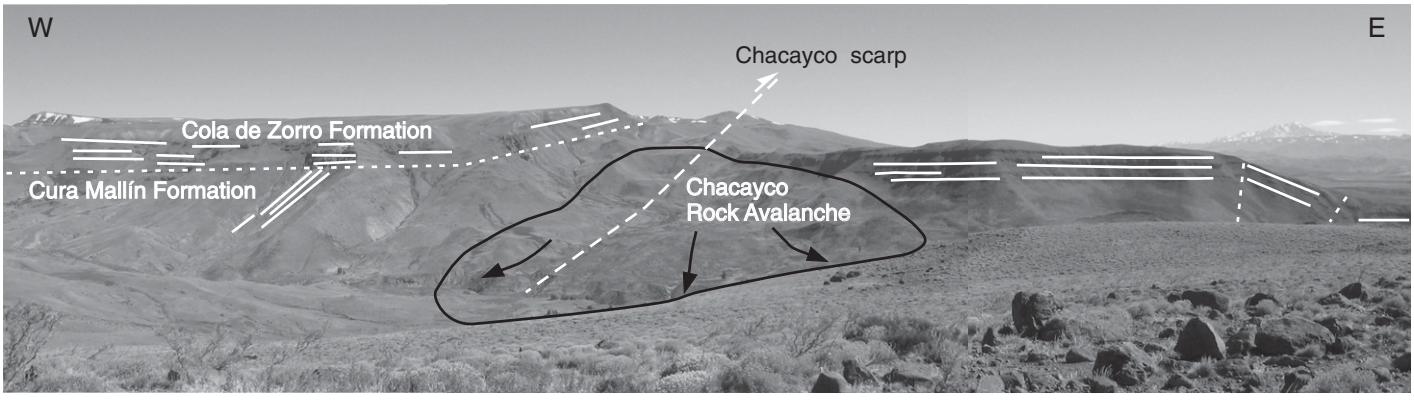

Figure 7. Structural control in the emplacement of the Chacayco rock avalanche, the headscarp of which developed in outcrops of the Cola de Zorro and Cura Mallín Formations.

Geological Society of America Bulletin, published online on 24 June 2011 as doi:10.1130/B30399.1

(Fig. 3). Therefore we redefined these deposits as rotational rockslides. Their headscarps developed in flat-lying volcanic rocks, and the massive deposits are poorly broken up, but contain a succession of inverse-facing scarps dissecting the deposit in several blocks (Fig. 3). The rockslide on the NW slope involved 340 × 10^6 m^3 of rock deposited over an area of 7.85 km^2. The juxtaposed deposit involved 1890 × 10^6 m^3 of rock that are spread over an area of 19.2 km^2 (Table 2; Fig. 3). Considering the good degree of preservation of juvenile morphologies, we estimate a postglacial age (<27 ka) for these deposits.

Rock-Slope Failures Not Coinciding with Tectonic Structures

Smaller rockslide deposits with volumes ranging from 1.6 × 10^5 to 50 × 10^5 m^3, which do not occur in the vicinity of any active fault or fold, were also mapped in the Reñileuvú and Ñireco valleys (Table 2; Fig. 3). Four of them are located in the Reñileuvú valley, in the surroundings of the Chochoy Mallín rock avalanche. These are rotational rockslides related to concave failure planes. Cosmogenic ^{3}He and ^{21}Ne dating of two boulders on the rotational slide located next to the distal part of the Chochoy Mallín rock avalanche deposit (named Chochoy I here) yielded ages of 29.9 ± 2.0 and 29.7 ± 2.0 ka, respectively (Table 3; means of ^{3}He and ^{21}Ne), or a mean age of 29.8 ± 1.4 ka for the slide.

González Díaz and Folguera (2005) classified two rockslides in the Ñireco valley (Fig. 3) as rock avalanches, based on volumes >10^6 m^3. The Lauquén Mallín slide (170 × 10^6 m^3) originated from the collapse of the southern slope of the valley (Table 2; Fig. 3). This deposit is characterized by intact blocks several hundreds of meters long with well-preserved stratification. The blocks are dissected by internal scarps. The stratification is back tilted in comparison with the original horizontal stratification on the slope. Only along the easternmost extension the blocks are broken up into a chaotic block field. Therefore we redefine this deposit as a rotational rockslide that decomposed only in its frontal part as a flow-like deposit. The rockslide deposit has dammed the valley, forming the 3-km-long Lauquén Mallín lake. We dated two samples from the frontal boulder deposit and obtained ^{3}He ages of 6.23 ± 0.63 and 6.55 ± 0.47 ka (Table 3), or a weighted mean of 6.44 ± 0.38 ka for the slide.

The second rockslide developed on the northern margin of the valley. The deposit is a nearly intact block with the stratification dipping ~40° toward the valley. Because the original stratification is also horizontal along this valley segment, the dip of the block indicates a forward rotation. The base of the block lies in the Lauquén Mallín lake; however, above water level, the block has a surface of 670 m^2. Between the block and the valley slope, there is an area partly covered by boulders up to several meters in diameter. We dated this boulder deposit with two ^{3}He ages of 6.41 ± 0.66 and 7.05 ± 0.80 ka (Table 3) to a mean of 6.67 ± 0.51 ka.

DISCUSSION

We have mapped all rockslides between the Guañacos and Picún-Leo valleys at the transition from the Central Andes to the Patagonian Andes in Argentina (Table 2; Fig. 3). The locations and sizes of 19 rockslides clearly show that they are not randomly distributed. All rockslides occurred along valleys eroded into a volcanic plateau. Among the total of rockslides two subgroups with distinctive characteristics can be defined: (1) rockslides lying along neotectonic structures and (2) rockslides lying in valley segments not affected by neotectonic deformation. In the following we discuss the location and timing of the rockslides in relation to their position toward the neotectonic structure and the structural type, and in a final step, we evaluate possible landslide-trigger mechanisms.

Temporal Distribution of Rockslides

We have dated six out of the 19 rockslide deposits described by surface-exposure dating using the cosmogenic nuclides ^{3}He and ^{21}Ne (Tables 2 and 3). The ages of the remaining 13 deposits have been relatively assessed by means of geomorphic indicators and stratigraphic relations with glacial deposits. Cosmogenic nuclide ages generally agree well within uncertainty limits, both between the two nuclides and the two boulders that were dated in each case, and are consistent with the geomorphic overprint of the deposit (Table DR3 [see footnote 1]). This suggests that the mean ages shown in Table 2 are close to the real ages of the events. Including the relative ages, we can divide the rockslide deposits in four groups: (1) older than 27 ka, (2) unspecified younger than 27 ka, (3) between 27 ka and 15–10 ka, and (4) younger than 15–10 ka (Table 2).

(1) Rockslides older than 27 ka include the Chochoy I slide and the Chochoy Mallín rock avalanche, which were both dated by cosmogenic nuclides (Table 3). The Chochoy Mallín rock avalanche is the only dated deposit for which the two ages do not overlap within uncertainties. This might be either the result of preexposure of one of the samples prior to landsliding, resulting in an age that is too old, or could be due to later tilting of a block, resulting in an age too young. In any case, the rock avalanche occurred ≥31.4 ka ago, which is the lower error limit of the lower ^{3}He age (Table 3). This fits well with the advanced stage of drainage development on the rock avalanche surface (Table DR3 [see footnote 1]). Therefore this rock avalanche is older than the last glacial maximum (~27 ka). Likewise, the weighted mean age of 29.8 ± 1.4 ka for the Chochoy I slide is somewhat older than the last glacial maximum. Both the Chochoy I slide and the Chochoy Mallín rock avalanche deposits lie below the lower limit of valley glaciations during maximum glacial extent (Fig. 3). We cannot exclude that further rock-slope failures have occurred in the glaciated part of the valleys >27 ka ago; however, their deposits would have been obliterated from the stratigraphic record.

(2) Rockslides unspecified younger than 27 ka are all deposits in valley sections glaciated during the last glacial maximum, which do, however, not show any signs of glacial overprint. This is the largest group, and most of them have juvenile surfaces suggesting even Holocene ages. However, due to the absence of any additional stratigraphic information, it is in most cases impossible to estimate a more precise age. Therefore most of the cosmogenic nuclide ages reported here were obtained for this group (see below).

(3) Rockslides between 27 ka and 15–10 ka: The Piche Moncol rock avalanche and the Guañacos I rotational slide deposits do not show any signs of glacial overprint of their morphology along the valley. However, they are covered by minor glacial deposits in elevations above 2000 m, indicating that they occurred sometime between the maximal glacial extent in the region (~27 ka) and a minor mountain glaciation thereafter. We consider that the altitudinal restriction of minor moraine deposits is related to the minor-scale glacial stage that occurred between 15 and 10 ka (Rabassa et al., 2005; Zech et al., 2008).

(4) Rockslides younger than 15–10 ka are abundant in the study area. All rockslide deposits dated by cosmogenic nuclides in the glaciated valleys have Holocene ages (Table 3). When comparing the surface morphology of undated and dated rock avalanches, the juvenile characteristics such as the drainage development (Table DR3 [see footnote 1]) are similar, suggesting that also the Cerro Guañacos and Laguna Negra rock avalanche deposits are of Holocene age. This is further supported by the absence of any deposits indicating glaciation of the mountain top of the Cerro Guañacos rock avalanche scar. This scar is located between the

Geological Society of America Bulletin, published online on 24 June 2011 as doi:10.1130/B30399.1

Piche Moncol and the Guañacos I slide scars and has the same altitude, but unlike the latter ones, no glacial deposits cover the scar area.

In contrast to other regions where landslide ages cluster close after deglaciation (Evans and Clague, 1994; Blikra et al., 2006; Cossart et al., 2008), all rockslides with a defined age in our study area postdate glaciation by more than 20,000 years (Table 2). Hence debuttressing by glacial retreat does not seem to be an important triggering mechanism. However, from a total of 19 rockslides, 11 are located above the boundary of the last glacial maximum, in sections with the greatest relief (Fig. 8A). This shows a correlation between relief produced by glacial and fluvial incision, and occurrence of rockslides.

Potential Causes for Landsliding

Most surprisingly, local relief is not the main control for the location and size of the rockslides (Fig. 8), and some rockslides with volumes in excess of 1×10^9 m^3 have even occurred in areas with relief below 700 m (Fig. 8), defined by Korup et al. (2007) as subcritical for the formation of $>10^8$ m^3 landslides. Although relief produced by erosion (up to 1000 m) significantly exceeds the relief produced by neotectonic activity (up to 400 m), most rockslides nucleate along interceptions of neotectonic structures with valleys (Table 2). This reflects that relief originated by glacial and fluvial erosion did not condition the movements by itself, and the tectonic deformation of the rocks, intensely fracturing the materials, was necessary to promote their collapse. Besides, for tectonic-related rockslides, we will show that the main control of the volume is the type of the structure, suggesting that tectonic deformation is the main conditioning factor for rocksliding (Fig. 8B).

Among the 19 rockslides, 13 coincide with neotectonic structures. They add up to a total rockslide volume of more than 10 km^3, while the six remaining rockslides are not associated with neotectonic structures and add up to less than 0.25 km^3. Among the 13 rockslides coinciding with neotectonic structures, those coinciding with folds are the most frequent and the largest ones. Nine rockslides with a total volume of >8.9 km^3 occur along folds—four of them along the Moncol anticline, which is the only fold with a regional extent, while the other five remaining rockslides occur along secondary structures. The Moncol anticline accounts for only 15% of the total shortening of all structures in the area. Eighty-five percent of the shortening in the area is accommodated by the El Convento, Chacayco, Guañacos, and Chochoy Mallín faults. Along those structures, four rockslides occurred with a total volume of

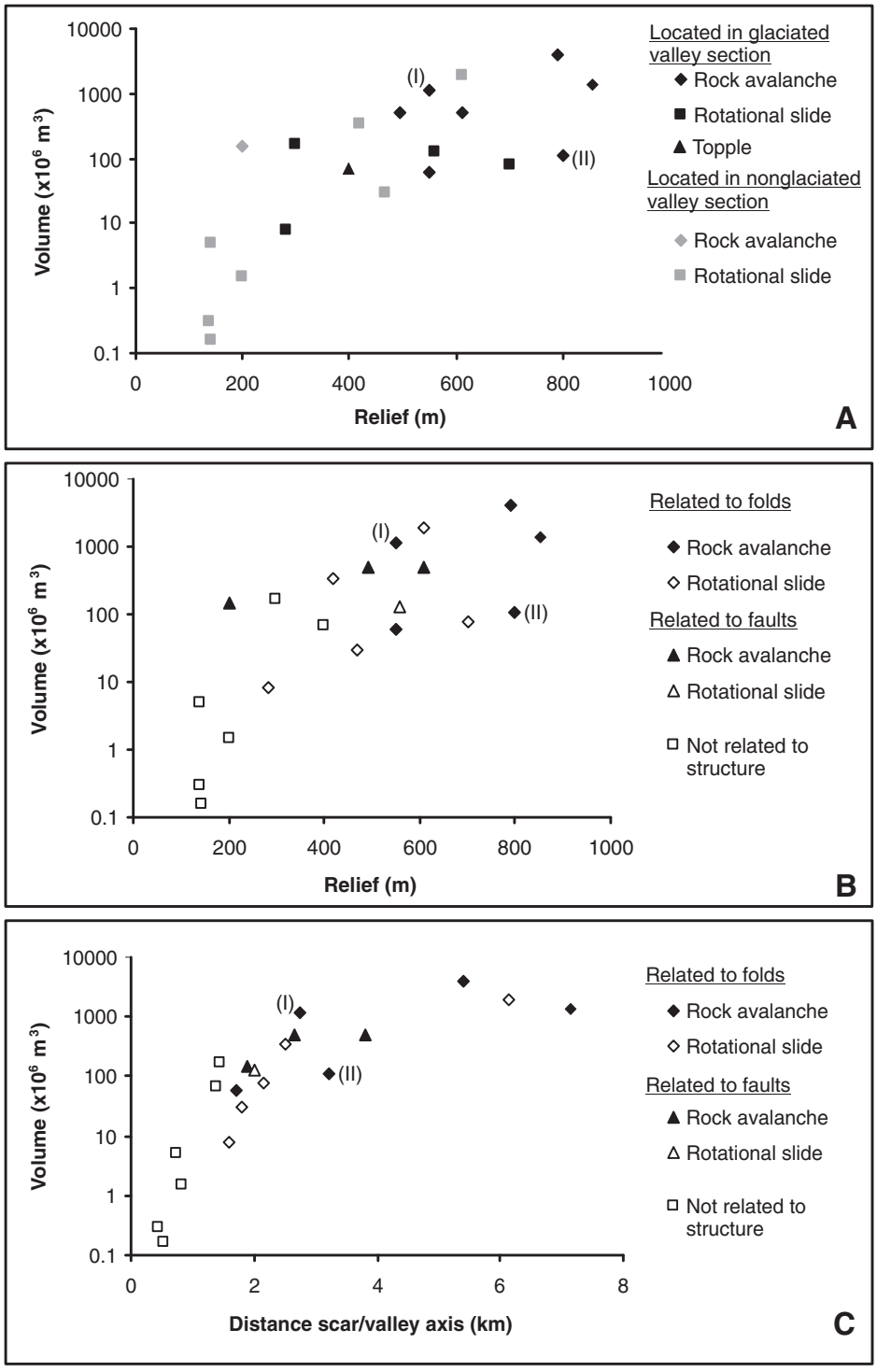

Figure 8. (A) Relationship between valley morphology (local relief) and volume of the rockslides, discriminated by location in glaciated or nonglaciated valley sections during last glacial maximum. (B) Relationship between local relief and volume of rockslides discriminated by type of neotectonic structure. (C) Relationship between volume of the rockslides and extension of headscarps discriminated by type of neotectonic structure. Volume axis is in logarithmic scale. (I) and (II) represent Cerro Guañacos parts I and II, respectively.

1.25 km^3. When comparing the total displacement along the faults with the volume of the rockslides initiated at them, a strong correlation is visible (Tables 1 and 2), with the Chacayco fault having 3.55 km of displacement and 1 km^3 of related rockslide material being the most dominant thrust fault that controls rockslides. It is followed by the Chochoy Mallín fault with 1.1-km displacement and 0.15 km^3 of rockslide material and the El Convento fault with 0.6-km total displacement and 0.13 km^3 of rockslide material. An exception is the Guañacos fault; this fault has a displacement of 2.5 km, but no rockslide is associated to its trace, which might be due to its position east of the valley glaciation boundary and hence coinciding with the area not affected by glacial slope oversteepening.

These observations show impressively that not only valley incision and hillslope denudation by erosion is governed by fracturing of rock along active structures on an orogenic scale, as argued by Molnar et al. (2007), but that fracture processes are related to the amount and, more importantly, to the style of deformation preconditioning slopes for rockslides. This also becomes nicely visible when comparing the distance from the rockslide scar to the valley axis (Fig. 8C). All rockslides not associated to any neotectonic structure have a headscarp stepping back into the slope for only 0.44–1.45 km (average at 0.9 km), while rockslides along neotectonic structures have affected areas of the slope stepping back from the valley axis between 1.7 and 7.1 km (average at 3.2 km; Table 2; Fig. 8C).

The average relief between headscarp and valley bottom is 220 m for the rockslides that are not located along any neotectonic structure, while for rockslides coinciding with neotectonic structures, it is 560 m. Almost all rock avalanches occurred in relief higher than 500 m (Fig. 8B). This is in agreement with the suggestion of Hermanns and Strecker (1999) in NW Argentina that the relief necessary to form rock avalanches must exceed 400 m. An exception is the Chochoy Mallín rock avalanche lying on the Chochoy Mallín fault, which occurred in a segment of the Reñileuvú valley with relief of 200 m, but the scar is nearly 2 km away from the valley axis. This confirms that in tectonically conditioned rockslides the zone of instability reaches farther back into the plateau and suggests that the threshold relief for the formation of rock avalanches depends on the extent to which rocks have been fractured prior to sliding. In valleys with slopes >25°, as is the case of our study area (~30°), Keefer (1984) suggested that the threshold can be as low as 150 m for intensely fractured rock slopes.

Interestingly, the ratios of local relief to distance between scar and valley axis are between 0.10 and 0.25 for the rock avalanches studied here, similar to the Fahrböschung of rock avalanches in other regions of the Andes and the world (Hungr and Evans, 1996; Hermanns and Strecker, 1999). This indicates that breakdown of rock material did not necessarily occur during sliding, but by tectonic fracturing prior to sliding, and that the entire rock mass did not move over long distances. This is supported by the fact that most of the larger rock avalanches stopped when reaching the valley bottom, with limited movement parallel to the valley floor (Fig. 3). Exceptions are the Cerro Guañacos and Chacayco rock avalanches, which are related to a runup of 90 and 80 m at the opposite valley slopes, respectively, indicating high mobility.

Triggering Mechanism

The distribution of rockslide ages between pre-LGM and Holocene, the volumes involved, the coincidence of the most voluminous rockslides with neotectonic structures, and the headscarps developed up to 7.1 km into the plateau indicate that climatic triggering is rather unlikely. The Cola de Zorro Formation (top dated at 1.7 ± 0.2 Ma by Folguera et al., 2004) and its sedimentary coverage were displaced 400 m in the Chacayco fault, 30 m in the Guañacos fault, and 15 m in the Chochoy Mallín fault. Also, three wind gaps developed over the Vilú Mallín anticline. This evidence and the records of local crustal earthquakes could be suggesting that repeated earthquakes rupturing the surface may have occurred on most of the structures in the past 1.7 million years. The Chacayco rock avalanche, the Lauquén Mallín rotational slide, and the Lauquén Mallín topple have identical ages within uncertainty limits. The Chacayco rock avalanche originated on the fault trace of the Chacayco fault, and the Lauquén Mallín slides occurred only a few kilometers east of it (Fig. 3). This suggests that these rockslides may have been triggered simultaneously and in a similar way to rock avalanches on the Denali fault in 2004 (Jibson et al., 2006), by an earthquake on the fault itself. This hypothesis is supported by recent seismic activity in the area. The estimated epicenters of the 1960 (9.5 Mw) earthquake in Chile, which has been the strongest instrumentally recorded earthquake on Earth, lie between 150 and 370 km SW from our study area (Plafker and Savage, 1970; Lorenzo-Martín et al., 2006 and references therein). However, no rockslides have been reported during this event in Argentina. Similarly, no voluminous rockslides were reported in the Andes related to the 27 February 2010 subduction earthquake in Chile. Therefore it is more likely that local crustal earthquakes with recurrence times exceeding human records have induced ground motion causing those rockslides, but aided by a favorable morphotectonic setting caused by alpine glaciers and fluvial incision that exposed the deformation zones of the neotectonic structures.

CONCLUSIONS

We have presented investigations of the eastern slope of the transitional area between the Central and Patagonian Andes, showing that neotectonic activity is going on and that important relief offsets in the Quaternary deposits have been produced along multiple structures. Headscarps of rockslides located along the path of neotectonic structures are several kilometers away from the valley axis. Due to the absence of any major structures conditioning these slopes to fail, this suggests that pre-fracturing of rocks during deformation is one of the main conditioning factors for massive rock-slope failures. For the total amount of rockslide material produced, the type of tectonic deformation is the first-order control, indicating that folding causes by far more preconditioning of rocks for failure than thrust faulting. This first-order control is followed by the amount of deformation accommodated along the structure. However, local relief due to alpine glaciation and fluvial incision is a further conditioning factor for such voluminous rockslides. The rockslides that occurred along valley sections not affected by neotectonic structures are several magnitudes smaller, and the style of sliding is rotational or toppling, highlighting the importance of the breakdown of rock bodies by neotectonic activity prior to sliding.

Rockslide ages are rather random, from older than the last glacial maximum to the mid Holocene, suggesting that climatic variability in this part of the Andes has played a minor role in triggering rockslides. However, three rockslides lying on or close to one of the major active faults have ages that agree within error limits, suggesting that they may have been triggered by a single crustal earthquake and that such events must have long recurrence times along that fault.

ACKNOWLEDGMENTS

The authors would like to thank Sanda Ortiz Ávila, Claudia Valdés Durán, Federico Ghiglione, José F. Mescua, and Ana Tedesco for field assistance and fruitful discussions. We also acknowledge Sergio Daicz for computational assistance, Enzio Schnabel for noble gas analyses, Sabine Tonn for major element determination of the pyroxenes by inductively coupled plasma–atomic emission spectrometry, and Knut Hahne and Heike Rothe for U and Th determinations by ICP-MS. The authors gratefully acknowledge Dr. Victor Ramos for the useful revision of the manuscript and assistance with the structural analysis. Careful and constructive reviews by F. Audemard and

C. Costa are gratefully acknowledged. We also thank J.M. Dortch and R. Arrowsmith for useful comments on an earlier version of this manuscript. Ivanna Penna was supported by a fellowship from National Scientific and Technical Research Council (CONICET). In addition the project received support by the Multinational Andean Project "Geosciences for Andean Communities" financed by the Canadian International Development Agency, by the Research Council of Norway through the International Center of Geohazards (ICG), and by GFZ Potsdam. This is ICG contribution 283 and Instituto de Estudios Andinos Don Pablo Groeber contribution R-16.

REFERENCES CITED

Abele, G., 1974, Bergstürze in den Alpen: Wissenschaftliche Alpenvereinshefte, München: Ausschüsse des Deutschen und Österreichischen Alpenvereins, v. 25, p. 231.

Antinao, J.L., and Gosse, J., 2009, Large rockslides in the Southern Central Andes of Chile (32°–34.5°S): Tectonic control and significance for Quaternary landscape evolution: Geomorphology, v. 104, p. 117–133, doi: 10.1016/j.geomorph.2008.08.008.

Ballantyne, C.K., Stone, J.O., and Fifield, L.K., 1998, Cosmogenic Cl-36 dating of postglacial landsliding at The Storr, Isle of Skye, Scotland: The Holocene, v. 8, p. 347–351, doi: 10.1191/095968398666797200.

Bermúdez, A., and Delpino, D., 1999, Erupciones subglaciales y en contacto con hielo en la región volcánica de Copahue, Neuquén: Salta, Argentina, Proceedings Congreso Geológico Argentino, XIV, v. 2, p. 250–253.

Blard, P.H., and Farley, K.A., 2008, The influence of radiogenic ^{4}He on cosmogenic ^{3}He determinations in volcanic olivine and pyroxene: Earth and Planetary Science Letters, v. 276, p. 20–29, doi: 10.1016/j.epsl.2008.09.003.

Blikra, L.H., Longva, O., Braathen, A., Anda, E., and Dehls, J.F., 2006, Rock slope failures in Norwegian fjord areas: Examples, spatial distribution and temporal pattern, *in* Evans, S.G., Scarascia Mugnozza, G., Strom, A.L., and Hermanns, R.L., eds., NATO Science Series IV: Earth and Environmental Sciences, v. 49, p. 475–496.

Bohm, M., Lüth, S., Echtler, H., Asch, G., Bataille, K., Bruhn, C., Rietbrock, A., and Wigger, P., 2002, The Southern Andes between 36° and 40°S latitude: Seismicity and average seismic velocities: Tectonophysics, v. 356, no. 4, p. 275–289, doi: 10.1016/S0040-1951(02)00399-2.

Brideau, M.A., Stead, D., Kinakin, D., and Fecova, K., 2005, Influence of tectonic structures on the Hope Slide, British Columbia, Canada: Engineering Geology, v. 80, no. 3, p. 242–259, doi: 10.1016/j.enggeo.2005.05.004.

Cossart, E., Braucher, R., Fort, M., Bourlès, D.L., and Carcaillet, J., 2008, Slope instability in relation to glacial debuttressing in alpine areas (Upper Durance catchment, southeastern France): Evidence from field data and ^{10}Be cosmic ray exposure ages: Geomorphology, v. 95, no. 1–2, p. 3–26, doi: 10.1016/j.geomorph.2006.12.022.

Costa, C.H., and González Díaz, E.F., 2007, Age constraints and paleoseismic implication of rock-avalanches in the Northern Patagonian Andes, Argentina: Journal of South American Earth Sciences, v. 24, no. 1, p. 48–57, doi: 10.1016/j.jsames.2007.03.001.

Costa, C.H., Audemard, F.A., Bezerra, F.H.R., Lavenu, A., and Machette, M.N., 2006, An overview of the main quaternary deformation of South America: Revista de la Asociación Geológica Argentina, v. 61, no. 4, p. 461–479.

Dahlstrom, C.D., 1969, Balanced cross sections: Canadian Journal of Earth Sciences, v. 6, p. 743–757.

Digregorio, J.H., and Uliana, M.A., 1975, Plano Geológico de la Provincia del Neuquén: Escala 1:500.000: Buenos Aires, Argentina, Proceedings Congreso Ibero-Americano de Geología Económica, II, v. 4, p. 69–93.

Dixon, H.J., Murphy, M.D., Sparks, S.J., Chávez, R., Naranjo, J.A., Dunkley, P.N., Young, S.R., Gilbert, J.S., and Pringue, M.R., 1999, The geology of Nevados de Chillán volcano, Chile: Revista Geológica de Chile, v. 26, no. 2, p. 227–253.

Dortch, J.M., Owen, L.A., Haneberg, W.C., Caffee, M.W., Dietsch, C., and Kamp, U., 2009, Nature and timing of large landslides in the Himalaya and Transhimalaya of northern India: Quaternary Science Reviews, v. 28, no. 11–12, p. 1037–1054, doi: 10.1016/j.quascirev.2008.05.002.

Escosteguy, L.D., Geuna, S.E., and Fauqué, L., 1999, La avalancha de rocas del Moncol, Cordillera Principal (Provincia de Neuquén, República Argentina): Salta, Argentina, Proceedings Congreso Geológico Argentino, XIV, v. 2, p. 67–70.

Evans, S.G., and Clague, J.J., 1994, Recent climatic change and catastrophic geomorphic processes in mountain environments: Geomorphology, v. 10, p. 107–128, doi: 10.1016/0169-555X(94)90011-6.

Fenton, C.R., Niedermann, S., Goethals, M.M., Schneider, B., and Wijbrans, J., 2009, Evaluation of cosmogenic ^{3}He and ^{21}Ne production rates in olivine and pyroxene from two Pleistocene basalt flows, western Grand Canyon, Arizona, USA: Quaternary Geochronology, v. 4, p. 475–492, doi: 10.1016/j.quageo.2009.08.002.

Folguera, A., and Ramos, V.A., 2002, Partición de la deformación durante el Neógeno en los Andes Patagónicos Septentrionales (37°-46°S): Revista de la Sociedad Geológica de España, v. 15, no. 1–2, p. 81–94.

Folguera, A., Ramos, V.A., Hermanns, R.L., and Naranjo, J., 2004, Neotectonics in the foothills of the southernmost central Andes (37°–38°S): Evidence of strike-slip displacement along the Antiñir-Copahue fault zone: Tectonics, v. 23, TC 5008, 23 p., doi: 10.1029/2003TC001533.

Folguera, A., Ramos, V.A., González Díaz, E., and Hermanns, R., 2006, Miocene to Quaternary deformation of the Guañacos fold-and-thrust belt in the Neuquén Andes between 37° and 37° 30´S, *in* Kay, S.M., and Ramos, V.A., eds., Late Cretaceous to Recent Magmatism and Tectonism of the Southern Andean Margin at the Latitude of the Neuquén Basin (36°–39°S): Geological Society of America Special Paper, v. 407, p. 247–266.

Goehring, B.M., Kurz, M.D., Balco, G., Schaefer, J.M., Licciardi, J., and Lifton, N., 2010, A reevaluation of in situ cosmogenic ^{3}He production rates: Quaternary Geochronology, v. 5, p. 410–418, doi: 10.1016/j.quageo.2010.03.001.

González Díaz, E.F., and Folguera, A., 2005, El reconocimiento de avalanchas de roca y deslizamientos de bloques rocosos prehistóricos en el área andina de Neuquén (37°15´ y 37°30'S): Revista de la Asociación Geológica Argentina, v. 60, no. 3, p. 446–460.

González Díaz, E.F., Folguera, A., Costa, C.H., Wright, E., and Elisondo, M., 2006, Los grandes deslizamientos de la región septentrional neuquina entre los 36° y los 38°S: Una propuesta de inducción sísmica: Revista de la Asociación Geológica Argentina, v. 61, no. 2, p. 197–217.

Hermanns, R.L., and Strecker, M.R., 1999, Structural and lithological controls on large Quaternary rock avalanches (sturzstroms) in arid northwestern Argentina: Geological Society of America Bulletin, v. 111, no. 6, p. 934–948, doi: 10.1130/0016-7606(1999)111<0934:SALCOL>2.3.CO;2.

Hermanns, R.L., Niedermann, S., Villanueva Garcia, A., Sosa Gomez, J., and Strecker, M.R., 2001, Neotectonics and catastrophic failure of mountain fronts in the southern intra-Andean Puna Plateau, Argentina: Geology, v. 29, no. 7, p. 619–622, doi: 10.1130/0091-7613(2001)029<0619:NACFOM>2.0.CO;2.

Hermanns, R.L., Naumann, R., Folguera, A., and Pagenkopf, A., 2004a, Sedimentologic analysis of deposits of a historic landslide dam failure in Barrancas valley causing a catastrophic 1914 Río Colorado flood, northern Patagonia, Argentina, *in* Lacerda, W.A., Ehrlich, M., Fontoura, S., and Sayao, A., eds., Landslides: Evaluation and Stabilization: Balkema, v. 2, p. 1439–1445.

Hermanns, R.L., Niedermann, S., Ivy-Ochs, S., and Kubik, P.W., 2004b, Rock avalanching into a landslide-dammed lake causing multiple dam failure in Las Conchas valley (NW Argentina)—Evidence from surface exposure dating and stratigraphic analyses: Landslides, v. 1, no. 2, p. 113–122, doi: 10.1007/s10346-004-0013-5.

Hermanns, R.L., Niedermann, S., Villanueva Garcia, A., and Schellenberger, A., 2006, Rock avalanching in the NW Argentine Andes as a result of complex interactions of lithologic, structural and topographic boundary conditions, climate change and active tectonics, *in* Evans, S.G., Scarascia Mugnozza, G., Strom, A., and Hermanns, R.L., eds., Landslides from Massive Rock Slope Failure: Netherlands, North Atlantic Treaty Organization Science Series, Springer, v. 49, p. 497–520.

Hermanns, R.L., Folguera, A., Penna, I.M., Fauqué, L., and Niedermann, S., 2011, Landslide dams in the Central Andes of Argentina (northern Patagonia and the Argentine northwest), *in* Evans, S.G., Hermanns, R.L., Strom, A., and Scarascia Mugnozza, G., eds., Lecture Notes in Earth Sciences: Natural and Artificial Rockslide Dams: Berlin, Springer, v. 133, p. 145–174 (in press).

Hovius, N., Stark, C.P., Tutton, M.A., and Abbott, L.D., 1998, Landslide-driven drainage network evolution in a pre–steady-state mountain belt: Finisterre Mountains, Papua New Guinea: Geology, v. 26, no. 12, p. 1071–1074, doi: 10.1130/0091-7613(1998)026<1071:LDDNEI>2.3.CO;2.

Hulton, N.R., Sugden, D., Payne, A., and Clapperton, C., 1994, Glacier modeling and the climate of Patagonia during the Last Glacial Maximum: Quaternary Research, v. 42, no. 1, p. 1–19, doi: 10.1006/qres.1994.1049.

Hungr, O., and Evans, S.G., 1996, Rock avalanche runout prediction using a dynamic model, *in* Senneset, K., ed., Landslides: Proceedings of the Seventh International Symposium on Landslides: Trondheim, Norway, Rotterdam, Balkema, v. 1, p. 233–238.

Jibson, R.W., Harp, E.L., Schulz, W., and Keefer, D.K., 2006, Large rock avalanches triggered by the M 7.9 Denali fault, Alaska, earthquake of 3 November 2002: Engineering Geology, v. 83, no. 1–3, p. 144–160, doi: 10.1016/j.enggeo.2005.06.029.

Jordan, T., Burns, W., Veiga, R., Pángaro, F., Copeland, P., Kelley, S., and Mpodozis, C., 2001, Extension and basin formation in the Southern Andes caused by increased convergence rate: A Mid-Cenozoic trigger for the Andes: Tectonics, v. 20, p. 308–324, doi: 10.1029/1999TC001181.

Keefer, D.K., 1984, Landslides caused by earthquakes: Geological Society of America Bulletin, v. 95, p. 406–421, doi: 10.1130/0016-7606(1984)95<406:LCBE>2.0.CO;2.

Kendrick, E.C., Bevis, M., Smalley, R.F., Cifuentes, O., and Galban, F., 1999, Current rates of convergence across the Central Andes: Estimates from continuous GPS observations: Geophysical Research Letters, v. 26, no. 5, p. 541–544, doi: 10.1029/1999GL900040.

Korup, O., Clague, J., Hermanns, R.L., Hewitt, K., Strom, A.L., and Weidinger, J.T., 2007, Giant landslides, topography and erosion: Earth and Planetary Science Letters, v. 261, no. 3–4, p. 578–589, doi: 10.1016/j.epsl.2007.07.025.

Kounov, A., Niedermann, S., de Wit, M.J., Viola, G., Andreoli, M., and Erzinger, J., 2007, Present denudation rates at selected sections of the South African escarpment and the elevated continental interior based on cosmogenic ^{3}He and ^{21}Ne: South African Journal of Geology, v. 110, p. 235–248, doi: 10.2113/gssajg.110.2-3.235.

Lorenzo-Martín, F., Roth, F., and Wang, R., 2006, Inversion for rheological parameters from post-seismic surface deformation associated with the 1960 Valdivia earthquake, Chile: Geophysical Journal International, v. 164, no. 1, p. 75–87, doi: 10.1111/j.1365-246X.2005.02803.x.

Marshak, S., and Woodward, N., 1988, Introduction to cross-section balancing, *in* Marshak, S., and Mitra, G., eds., Basic Methods of Structural Geology: Englewood Cliffs, Prentice-Hall, p. 303–332.

Martino, S., Minutolo, A., Paciello, A., Rovelli, A., Scarascia Mugnozza, G., and Verrubbi, V., 2006, Evidence of amplification effects in fault zone related to rock mass jointing: Natural Hazards, v. 39, no. 3, p. 419–449, doi: 10.1007/s11069-006-0001-2.

Masarik, J., and Reedy, R.C., 1995, Terrestrial cosmogenic-nuclide production systematics calculated from numerical simulations: Earth and Planetary Science

Letters, v. 136, p. 381–395, doi: 10.1016/0012-821X(95)00169-D.

Masarik, J., and Wieler, R., 2003, Production rates of cosmogenic nuclides in boulders: Earth and Planetary Science Letters, v. 216, p. 201–208, doi: 10.1016/S0012-821X(03)00476-X.

Melnick, D., Bookhagen, B., Echtler, H., and Strecker, M., 2006, Coastal deformation and great subduction earthquakes, Isla Santa María, Chile (37°S): Geological Society of America Bulletin, v. 118, no. 11–12, p. 1463–1480, doi: 10.1130/B25865.1.

Molnar, P., Anderson, R.S., and Anderson, S.P., 2007, Tectonics, fracturing of rock, and erosion: Journal of Geophysical Research, v. 112, p. F03014, doi: 10.1029/2005JF000433.

Montgomery, D.R., and Brandon, M.T., 2002, Topographic controls on erosion rates in tectonically active mountain ranges: Earth and Planetary Science Letters, v. 201, p. 481–489, doi: 10.1016/S0012-821X(02)00725-2.

Niedermann, S., 2002, Cosmic-ray-produced noble gases in terrestrial rocks: Dating tools for surface processes: Reviews in Mineralogy and Geochemistry, v. 47, p. 731–784, doi: 10.2138/rmg.2002.47.16.

Niedermann, S., Bach, W., and Erzinger, J., 1997, Noble gas evidence for a lower mantle component in MORBs from the southern East Pacific Rise: Decoupling of helium and neon isotope systematics: Geochimica et Cosmochimica Acta, v. 61, p. 2697–2715, doi: 10.1016/S0016-7037(97)00102-6.

Pardo-Casas, F., and Molnar, P., 1987, Relative motion of the Nazca (Farallón) and South American Plates since Late Cretaceous time: Tectonics, v. 6, no. 3, p. 233–248, doi: 10.1029/TC006i003p00233.

Plafker, G., and Savage, J.C., 1970, Mechanism of the Chilean Earthquakes of May 21 and 22, 1960: Geological Society of America Bulletin, v. 81, no. 4, p. 1001–1030, doi: 10.1130/0016-7606(1970)81[1001:MOTCEO]2.0.CO;2.

Rabassa, J., and Clapperton, C.M., 1990, Quaternary glaciations of the Southern Andes: Quaternary Science Reviews, v. 9, p. 153–174, doi: 10.1016/0277-3791(90)90016-4.

Rabassa, J., Coronato, A., and Salemme, M., 2005, Chronology of the Late Cenozoic Patagonian Glaciations and their correlation with biostratigraphic units of the Pampean Region (Argentina): Journal of South American Earth Sciences, v. 20, no. 1–2, p. 81–103, doi: 10.1016/j.jsames.2005.07.004.

Redfield, T.F., and Osmundsen, P.T., 2009, The Tjellefonna fault system of Western Norway: Linking late-Caledonian extension, post-Caledonian normal faulting, and Tertiary rock uplift with the landslide-generated tsunami event of 1756: Tectonophysics, v. 474, no. 1–2, p. 106–123, doi: 10.1016/j.tecto.2009.02.006.

Schäfer, J.M., Ivy-Ochs, S., Wieler, R., Leya, I., Baur, H., Denton, G.H., and Schlüchter, C., 1999, Cosmogenic noble gas studies in the oldest landscape on earth: Surface exposure ages of the Dry Valleys, Antarctica: Earth and Planetary Science Letters, v. 167, no. 3–4, p. 215–226, doi: 10.1016/S0012-821X(99)00029-1.

Singer, B., Hildreth, W., and Vincze, Y., 2000, $^{40}Ar/^{39}Ar$ evidence for early deglaciation of central Chilean Andes: Geophysical Research Letters, v. 27, p. 1663–1666, doi: 10.1029/1999GL011065.

Somoza, R., and Ghidella, M.E., 2005, Convergencia en el margen occidental de América del Sur durante el Cenozoico: Subducción de las placas de Nazca, Farallón y Alluk: Revista de la Asociación Geológica Argentina, v. 60, no. 4, p. 797–809.

Stone, J.O., 2000, Air pressure and cosmogenic isotope production: Journal of Geophysical Research, v. 105, p. 23,753–23,759, doi: 10.1029/2000JB900181.

Strecker, M.R., and Marrett, R.A., 1999, Kinematic evolution of fault ramps and role in development of landslides and lakes in northwestern Argentine Andes: Geology, v. 27, p. 307–310, doi: 10.1130/0091-7613(1999)027<0307:KEOFRA>2.3.CO;2.

Suárez, M., and Emparán, C., 1995, The stratigraphy, geochronology, and paleophysiography of a Miocene fresh-water interarc basin, southern Chile: Journal of South American Earth Sciences, v. 8, no. 1, p. 17–31, doi: 10.1016/0895-9811(94)00038-4.

Suárez, M., and Emparán, C., 1997, Hoja Curacautín: Regiones de la Araucanía y del Bío Bío: Carta Geológica de Chile: Santiago, Servicio Nacional de Geología y Minería de Chile, v. 71, 105 p., scale 1:250,000, 1 sheet.

Svensson, H., 1959, Is the cross section of a glacial valley a parabola?: Journal of Glaciology, v. 3, no. 25, p. 362–363.

Tašárová, Z., 2004, Gravity data analysis and interdisciplinary 3D modelling of a convergent plate margin (Chile, 36°–42°S) [Ph.D. thesis]: Freie Universität Berlin, 169 p.

Trauth, M.H., Alonso, R.A., Haselton, K.R., Hermanns, R.L., and Strecker, M.R., 2000, Climate change and mass movements in the northwest Argentine Andes: Earth and Planetary Science Letters, v. 179, p. 243–256, doi: 10.1016/S0012-821X(00)00127-8.

U.S. Geological Survey (USGS)/National Earthquake Information Center (NEIC), 1973–present, Preliminary Determination of Epicenters (PDE) Catalog: http://neic.usgs.gov/neis/epic/.

Vergara, M.M., and Muñoz, J.B., 1982, La Formación Cola de Zorro en la Alta Cordillera Andina Chilena (36°-39° Lat. S), sus características petrográficas y petrológicas: Una revisión: Revista Geológica de Chile, no. 17, p. 31–46.

Vietor, T., and Echtler, H., 2006, Episodic Neogene southward growth of the Andean subduction orogen between 30°S and 40°S—Plate motions, mantle flow, climate, and upper-plate structure, *in* Oncken, O., Chong, G., Franz, G., Giese, P., Götze, H-J., Ramos, V.A., Strecker, M.R., and Wigger, P., eds., The Andes—Active Subduction Orogeny: Berlin, Frontiers in Earth Science Series, Springer-Verlag, v. 1, no. 18, p. 375–400.

Zech, R., May, J.-H., Kull, C., Ilgner, J., Kubik, P.W., and Veit, H., 2008, Timing of the late Quaternary glaciation in the Andes from ~15 to 40°S: Journal of Quaternary Science, v. 23, no. 6, p. 635–647, doi: 10.1002/jqs.1200.

Science Editor: Brendan Murphy
Associate Editor: Victor Ramos

Manuscript Received 23 August 2010
Revised Manuscript Received 15 November 2010
Manuscript Accepted 17 November 2010

Printed in the USA